Int J Earth Sci (Geol Rundsch) (2008) 97:739–764
DOI 10.1007/s00531-007-0188-9

ORIGINAL PAPER

Petrochemistry and petrology of I-type granitoids in an arc setting: the composite Torul pluton, Eastern Pontides, NE Turkey

Abdullah Kaygusuz · Wolfgang Siebel · Cüneyt Şen · Muharrem Satir

Received: 28 November 2006 / Accepted: 16 April 2007 / Published online: 22 May 2007

Abstract The Upper Cretaceous Torul pluton, located in the Eastern Pontides, is of sub-alkaline affinity and displays features typical of volcanic arc granitoids. It is a composite pluton consisting of granodiorite, biotite hornblende monzogranite, quartz monzodiorite, quartz monzonite and hornblende biotite monzogranite. The oldest syenogranite (77.9 ± 0.3 Ma) and the youngest quartz diorite form small stocks within the pluton. Samples from the granodiorites, biotite hornblende monzogranites, quartz monzodiorites, quartz monzonites and hornblende biotite monzogranites have SiO_2 between 57 and 68 wt% and display high-K calc-alkaline, metaluminous to peraluminous characteristics. Chondrite-normalized REE patterns are fractionated (La_{cn}/Lu_{cn} = 6.0–14.2) with pronounced negative Eu anomalies (Eu/Eu* = 0.59–0.84). Initial $\varepsilon_{Nd(i)}$ values vary between –3.1 and –4.1, initial $^{87}Sr/^{86}Sr$ values between 0.7058 and 0.7072, and $\delta^{18}O$ values between +4.4 and +7.3‰. The quartz diorites are characterized by relatively high Mg-number of 36–38, low contents of Na_2O (2.3–2.5 wt%) and SiO_2 (52–55 wt%) and medium-K calc-alkaline, metaluminous composition. Chondrite-normalized REE patterns are relatively flat [$(La/Yb)_{cn}$ = 2.8–3.3; $(Tb/Yb)_{cn}$ = 1.2] and show small negative Eu anomalies (Eu/Eu* = 0.74–0.76). Compared to the other rock types, radiogenic isotope signatures of the quartz diorites show higher $^{87}Sr/^{86}Sr$ (0.7075–0.7079) and lower $\varepsilon_{Nd(i)}$ (–4.5 to –5.3). The syenogranites have high SiO_2 (70–74 wt%) and display high-K calc-alkaline, peraluminous characteristics. Their REE patterns are characterized by higher La_{cn}/Lu_{cn} (12.9) and Eu/Eu* (0.76–0.77) values compared to the quartz diorites. Isotopic signatures of these rocks [$\varepsilon_{Nd(i)}$ = –4.0 to –3.3; $^{87}Sr/^{86}Sr_{(i)}$ = 0.7034–0.7060; δ^{18} O = + 4.9 to + 8.2] are largely similar to the other rock types but differ from that of the quartz diorites. Fractionation of plagioclase, hornblende, pyroxene and Fe–Ti oxides played an important role in the evolution of Torul granitoids. The crystallization temperatures of the melts ranged from 800 to 900°C as determined from zircon and apatite saturation thermometry. All these characteristics, combined with low K_2O/Na_2O, low $Al_2O_3/(FeO_T + MgO + TiO_2)$, and low $(Na_2O + K_2O)/(FeO_T + MgO + TiO_2)$ ratios suggest an origin through dehydration melting of mafic lower crustal source rocks.

Keywords Composite Torul pluton · Eastern Pontides · Granitoid · Isotope systematic · Petrogenesis

A. Kaygusuz (✉)
Department of Geology, Karadeniz Technical University, 29000 Gumushane, Turkey
e-mail: abdullah@ktu.edu.tr; abdullah.kaygusuz@gmail.com

W. Siebel
Institute of Geosciences, Universität Tübingen, Wilhelmstr. 56, 72074 Tübingen, Germany
e-mail: wolfgang.siebel@uni-tuebingen.de

C. Şen
Department of Geology, Karadeniz Technical University, 61080 Trabzon, Turkey
e-mail: csen@ktu.edu.tr

M. Satir
Institute of Geosciences, Universität Tübingen, Wilhelmstr. 56, 72074 Tübingen, Germany
e-mail: satir@uni-tuebingen.de

Introduction

Granitoid plutons are essential constituents of collision belts. They are characterized by a large compositional diversity arising from different source compositions, vari-

able melting conditions, and complex chemical and physical interactions between mafic and felsic magmas, fractional crystallization and crustal contamination (e.g. DePaolo 1981; Zorpi et al. 1991; Roberts and Clemens 1993; Galan et al. 1996; Thompson and Connolly 1995; Altherr et al. 1999, 2000; Altherr and Siebel 2002). There is a strong link between mineralogy, geochemical and isotopic composition and the geodynamic setting of granitoids. For this reason, compositionally well-characterized granitoids of known age may constrain the evolution and development of the continental crust through geological time (Barbarin 1999). Although numerous granitoid plutons have been extensively studied in terms of geochemistry and petrology, the transition from subduction to post-collisional extension still attracts attention and is often debated. The relationships among the stages of collision, the nature of the produced melts and their chemical composition are controversially discussed in magmatic provinces such as the Alpine-Himalayan orogenic belt. This belt embraces various arc, collision and post-collision geologic settings and magmatic rocks were formed during each of these settings. In the Alpine–Himalayan belt, Turkey as a zone of interaction between two major tectonic plates, Eurasia and Gondwanaland, lies in an important geodynamic position. The Pontide unit (Ketin 1966) of Turkey includes various eruptive and intrusive rocks, constituting the widespread Eastern Pontide Terrane, many of which are related to the convergence of these two plates (Fig. 1).

The Eastern Pontides (Ketin 1966), extending from the Black Sea coast to about 200 km south and straddling the North Anatolian Fault, form the northern margin of Anatolia (Fig. 1). The Eastern Pontides provide insight into paleo-island arc and long-term crustal evolution from pre-subduction rifting, through arc volcanism and plutonism to post-subduction alkaline volcanism (Akın 1978; Şengör and Yılmaz 1981; Akıncı 1984). The present-day geological setting of the Eastern Pontides is mainly the result of three main Neo-Tethyan volcanic cycles during the Jurassic, Upper Cretaceous and Eocene (Adamia et al. 1977; Eğin et al. 1979; Kazmin et al. 1986; Korkmaz et al. 1995; Çamur et al. 1996; Arslan et al. 1997, 2000). A number of studies (Tokel 1977; Akın 1978; Yılmaz 1981; Ercan and Gedik 1983; Robinson et al. 1995; Genç and Yılmaz 1995; Çamur et al. 1996; Yılmaz and Boztuğ 1997; Okay and Şahintürk 1997; Arslan et al. 1997; Şen et al. 1998) have stressed the different temporal, spatial and compositional relationships between the three Neo-Tethyan convergence systems.

In the Pontides of Turkey, particularly in the Eastern Pontides, the magmatic arc has been interpreted as related to the evolution of the Tethyan Ocean between Palaeozoic and Tertiary times (Şengör and Yılmaz 1981). In the western part of the Eastern Pontides, the Jurassic-Lower Cretaceous sequence has been interpreted to have formed during a rifting event and to indicate a passive continental margin, while during the Late Cretaceous both the eastern and western parts of the Eastern Pontides became an active

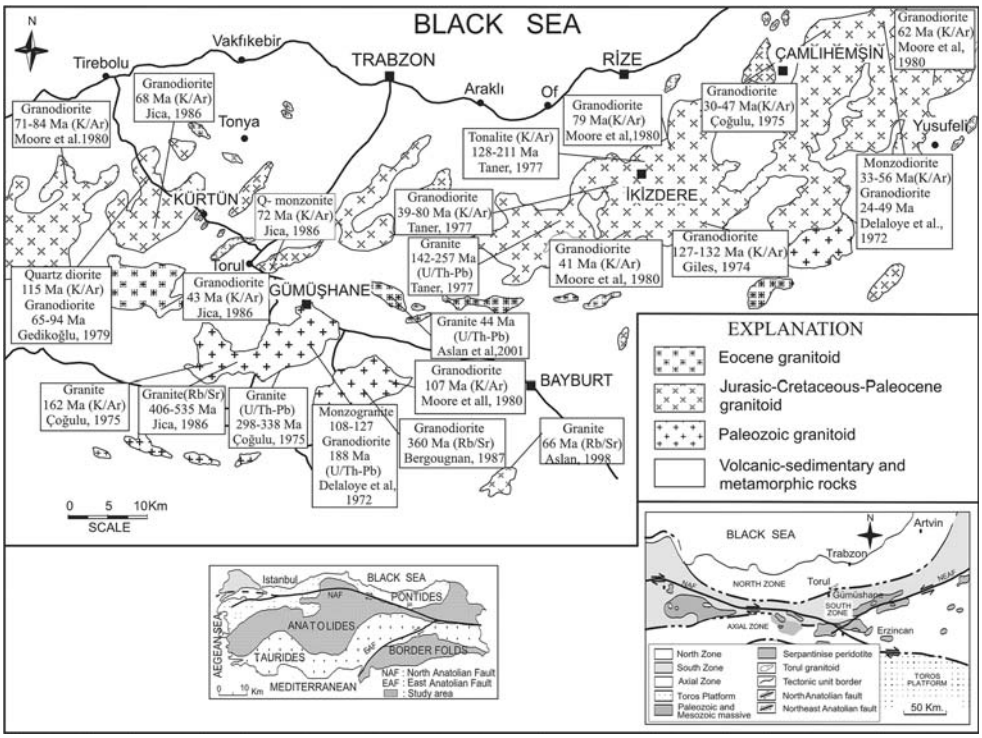

Fig. 1 Simplified map showing the main granitoid distribution in the Eastern Pontides (modified from Gedik at al. 1992 and Güven 1993). Tectonic map of Turkey (from Ketin 1966), and major structures of the Eastern Pontides

continental margin (Yılmaz et al. 2000). The collision of the Eastern Pontides island arc with the Anatolides-Taurides along the İzmir-Ankara-Erzincan Suture Zone in the south occurred during Palaeocene–Early Eocene compressional events (Okay and Şahintürk 1997; Kazmin et al. 2000). Subsequent regional extension, only a few million years following the collision, was associated with post-collisional magmatism in the Eastern Pontides.

Recent studies (Boztuğ et al. 2003, 2004, 2006) have identified intrusive units derived from different geodynamic environments, with different ages, compositions and emplacement levels in the crust. These range from Early Cretaceous (Delaloye et al. 1972; Giles, 1974; Taner, 1977; Gedikoğlu, 1978; Moore et al. 1980; Boztuğ et al. 2003) through Late Cretaceous (Taner, 1977; Moore et al. 1980; Jica, 1986; Okay and Şahintürk, 1997; Yılmaz et al. 1997; Kaygusuz 2000; Köprübaşı et al. 2000, Boztuğ et al. 2006) to Eocene (Karslı 2002; Arslan et al. 2004; Boztuğ et al. 2004; Şahin 2005; Topuz et al. 2005; Boztuğ et al. 2006) in age. Rocks comprise low-K tholeites (sometimes high-K), calc-alkaline metaluminous granitoids, peraluminous leucogranites, silica-oversaturated alkaline syenites and monzonites (Yılmaz and Boztuğ, 1996; Boztuğ et al. 2003) which formed during arc-collisional, syn-collisional crustal thickening and post-collisional extensional regimes (Yılmaz and Boztuğ, 1996; Okay and Şahintürk, 1997; Yılmaz et al. 1997; Boztuğ et al. 2003; Yeğingil et al. 2002). The Early/Late Cretaceous to Early Palaeocene arc-related granitoids have calc-alkaline, metaluminous I-type character, and show characteristics of magma mingling–mixing between coeval mafic and felsic magma sources (Okay and Şahintürk 1997; Yılmaz et al. 1997; Boztuğ et al. 2003). The syn-collisional granitoids, which intrude the arc-related granodiorites and granites, are biotite leucogranites with peraluminous S-type chemical and mineralogical compositions (Boztuğ et al. 2003). The Eocene post-collisional extension-related intrusive rocks form small stocks of diorites and quartz diorites/monzodiorites of calc-alkaline to tholeitic affinity, and syenites to monzonites of alkaline affinity (Yılmaz and Boztuğ 1996; Boztuğ et al. 2003; Arslan and Aslan 2005). In the Torul region of the Eastern Pontides, arc-related magmatism developed under a compressional regime and is characterized by the predominance of calc-alkaline granitoids.

In this paper, we present a comprehensive set of new geochemical, Sr, Nd and oxygen isotope data on the Torul pluton, eastern Pontide magmatic arc. This arc comprises several granitoid plutons of different sizes. Although some of the Eastern Pontide arc granitoids were geochemically studied and radiometrically dated (Fig. 1), not much work was done to constrain their magma sources and magma production processes.

Geological setting

The Eastern Pontides can be divided into three zones: the northern, southern and axial zones (Bektaş et al. 1999). These zones have different lithological characteristics and are separated by E–W, NE–SW and NW–SE oriented fault zones that define the block faulted tectonic style of the eastern Pontides (Bektaş and Çapkınoğlu 1997). The northern zone of the eastern Pontides contains extensive Upper Cretaceous and Tertiary volcanic rocks (Pontide magmatic arc) cropping out mainly along the Black Sea coast. Palaeozoic plutonic and metamorphic rocks and their sedimentary cover sequences characterize the southern zone. The top of the succession consists of Eocene sediments with volcanic lithoclasts and macro foraminifera. In the axial zone, Mesozoic Alpine type peridotites and gabbro-diorites occur.

The Torul pluton covers an area of approximately 40 km^2 and is an elliptical body with the long axes extending NE–SW. The pluton separates the southern and northern zone of the Eastern Pontides (Kaygusuz and Şen 1998) (Fig. 2). The southern zone comprises lower Jurassic volcanic and pyroclastic rocks at the bottom and Eocene volcanic rocks at the top. Cretaceous to Palaeocene sediments are intercalated into the volcanic series. The northern volcanic series is made up of Late Cretaceous basic and acidic volcanic rocks interbedded with sedimentary layers. According to field observations, the Torul pluton cuts upper Jurassic, early Cretaceous and late Cretaceous formations, and is cut by aplitic, dacitic and andesitic dykes (Kaygusuz 2000). A K–Ar age of 72.1 ± 3.6 Ma has been obtained for a quartz monzonite sample from the pluton (Jica 1986).

The Torul pluton is a composite pluton which can be subdivided into three major units. These units are, from oldest to youngest: (1) small stocks of syenogranites (77.9 ± 0.3 Ma, this study), (2) granodiorites, biotite hornblende monzogranites, quartz monzodiorites, quartz monzonites, hornblende biotite monzogranites (72.1 ± 3.6 Ma; Jica 1986), and, (3) small stocks of quartz diorites which cut the granodiorites and biotite hornblende monzogranites representing the youngest subunit within the Torul pluton. The syenogranites and the quartz diorites form small outcrops, whereas the granodiorites, biotite hornblende monzogranites, quartz monzodiorites, quartz monzonites and hornblende biotite monzogranite make up the main volume of the pluton (Fig. 2).

Analytical techniques

More than 300 samples were collected from the Torul Pluton. The modal mineralogy of 267 samples was deter-

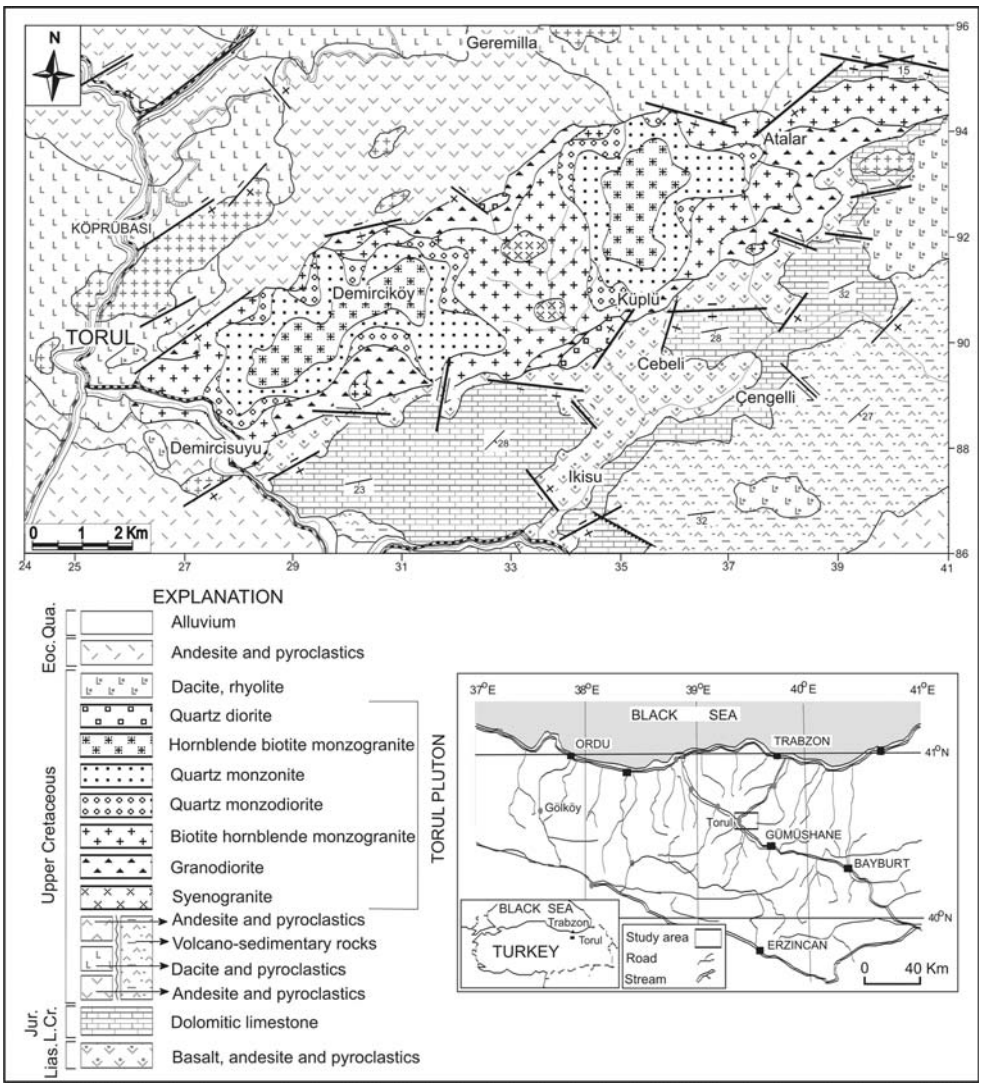

Fig. 2 Location and geological map of the investigated area (modified from Kaygusuz 2000)

mined by point counting with a Swift automatic counter fitted to a polarizing microscope. On each thin-section a total of 1,000–1,250 points were counted. Modes were normalized to 100% (Table 1).

After macroscopic and microscopic investigation, 65 samples were selected for major, trace and rare earth element analyses. Major and trace elements were determined by wavelength dispersive XRF at the Department of Geology, University of New Brunswick (Canada), by full automated energy dispersive XRF at the Geological Engineering Department, Karadeniz Technical University (Turkey), and by ICP-emission spectrometry and ICP-mass spectrometry at ACME, Analytical Laboratories Ltd., Vancouver (Canada), using standard techniques. Major and trace elements were analysed by ICP after 0.2 g of rock-powder was fused with 1.5 g $LiBO_2$ and dissolved in 100 ml 5% HNO_3. Loss on ignition (LOI) was determined on the dried samples heated at 1,000°C. Rare earth element analyses were performed by ICP-MS at ACME Analytical Laboratories Ltd., Vancouver. Detection limits range from 0.01 to 0.1 wt% for major oxides, from 0.1 to 10 ppm for trace elements, and from 0.01 to 0.5 ppm for the rare earth elements.

Mineral analyses were carried out at the University of New Brunswick (Canada) with a JEOL JSM-6400 scanning electron microscope equipped with a Link eXL energy dispersive analyser and a single wavelength dispersive channel. X-ray analyses were done at an acceleration potential of 15 kV and sample currents of 2.5 nA, using a live time of 100 s for energy dispersive data acquisition. Data were reduced with the Link ZAF procedure using a combination of mineral (orthoclase-K, albite-Na, hornblende-Al, olivine-Mg, pyroxene-Si, K, Ca) and metal (Fe, Ti) standards. Analytical results are presented in Tables 2 and 3. Detection limits are generally about 0.1 wt%.

Rb–Sr, Sm–Nd and oxygen isotope analyses were performed at the Institute of Geosciences, Tübingen. For the radiogenic isotope study, very fine grained (<10 μm)

Table 1 General petrographic features of the various rock-types from the Torul pluton

Rock unit	Syenogranite (n = 15)	Granodiorite (n = 44)	Bt-hbl-mg (n = 80)	Qtz-monzodiorite (n = 22)	Qtz-monzonite (n = 56)	Hbl-bt-mg (n = 52)	Qtz-diorite (n = 5)	MME (Qtz-mnzd, mnzd, Diorite) (n= 12)
Texture	Allotriomorphic	Hypidiomorphic–porphyritic	Hypidiomorphic	Hypidiomorphic	Hypidiomorphic	Hypidiomorphic–porphyritic	Hypidiomorphic–porphyritic	Hypidiomorphic–Allotriomorphic
Grain size	Fine	Fine to medium	Medium	Medium	Medium	Fine to medium	Fine	Fine
Modal min (%)	Min–max	Min–max	Min–max	Min–max	Min–max	Min–max	Min–max	Min–max
Plagioclase	10–23	38–59	31–46	43–54	28–47	24–41	55–59	44–65
K-Feldspar	43–53	7–24	21–34	16–27	24–40	23–44	3–4	2–16
Quartz	24–34	17–29	17–31	11–18	11–19	17–29	11–13	1–11
Biotite	2–7	0–9	0–6	0–6	0–7	2–11	–	1–10
Hornblende	0–3	0–14	1–13	5–19	1–16	0–7	15–19	15–28
Pyroxene	–	0–2	0–1	0–1	0–1	0–2	0–1	1–2
Mineral chemistry								
Plg (An%)	–	38–53	23–52	45–49	40–49	27–46	–	–
K-Feld (Or%)	–	74–94	87–89	72–73	91–96	88–93	–	–
Bt (Mg#)	–	0.6	0.5–0.7	0.7	0.6	0.6	–	–
Bt-TiO_2 (wt%)	–	4.3–6.1	5.2–5.4	5.7	4.7–5.5	5.1–5.6	–	–
Bt–Al^{IV} (pfu)	–	2.0–2.3	2.3–2.4	2.3	2.2–2.3	2.2–2.3	–	–
Hbl (Mg#)	–	0.7–0.9	0.7–0.8	0.8	0.7–0.8	0.7–0.8	–	–
Pyx (Wo%)	–	–	–	–	26–29	26–47	–	–
Accessory Phases	Sphene, allanite, zircon, opaques	Sphene, apatite, allanite, zircon, epidote, opaques	Sphene, apatite, allanite, zircon, epidote, opaques	Sphene, apatite, allanite, zircon, epidote, opaques	Sphene, apatite, allanite, zircon, epidote, opaques	Sphene, apatite, allanite, zircon, epidote, opaques	Allanite, apatite, opaques	Apatite, zircon, epidote, opaques
Secondary Minerals	Sericite, clay minerals	Sericite, carbonate, chlorite, clay minerals	Sericite, chlorite, clay minerals	Sericite, carbonate, chlorite, clay minerals	Sericite, chlorite, clay minerals	Sericite, chlorite, clay minerals	Sericite, carbonate, clay minerals	Carbonate, chlorite, clay minerals

n sample number, *min* minimum values, *max* maximum values, *Qtz* Quartz, *Bt* Biotite, *Hbl (hbl)* Hornblende, *Plg* Plagioclase, *K-feld* K-feldspar, *Pyx* Pyroxene, *MME* Mafic microgranular enclaves, *mnzd* Monzodiorite

Table 2 Microprobe analysis of plagioclase and K-feldspar from the Torul pluton

Rock types	Plagioclase					K-Feldspar				
	Granodiorite (n = 8) Min–max	Bt-hbl-monzogranite (n = 5) Min–max	Qtz-monzodiorite (n = 2) Min–max	Qtz-monzonite (n = 3) Min–max	Hbl-bt-monzogranite (n = 6) Min–max	Granodiorite (n = 5) Min–max	Bt-hbl-monzogranite (n = 2) Min–max	Qtz-monzodiorite (n = 2) Min–max	Qtz-monzonite (n = 3) Min–max	Hbl-bt-monzogranite (n = 5) Min–max
SiO_2	45.8–58.0	53.9–62.1	54.6–55.0	55.5–56.9	55.2–60.1	64.3–65.9	64.9–65.2	64.7–65.4	64.6–65.3	62.8–64.4
TiO_2	0.0	0.0–0.02	0.0–0.03	0.0	0.0	0.0–0.04	0.0–0.1	0.03–0.06	0.0–0.01	0.0–0.1
Al_2O_3	27.1–36.4	25.3–29.9	27.4–27.9	27.6–29.8	25.2–29.7	19.3–20.1	19.5–19.7	19.7–19.9	19.6–19.7	19.4–19.6
FeO	0.3–0.5	0.2–0.3	0.3–0.4	0.2–0.4	0.2–0.4	0.0–0.1	0.03	0.1	0.1	0.0
MnO	–	–	–	–	–	0.0	0.0	0.0	0.0–0.01	0.0–0.03
CaO	8.1–17.7	5.1–10.8	10.0–10.3	8.4–10.5	4.7–9.6	0.0–0.4	0.0	0.1–0.2	0.0–0.01	0.0
Na_2O	1.4–6.9	5.3–9.1	6.0–6.7	5.6–6.9	5.3–9.1	0.7–2.7	1.2–1.5	3.0–3.1	0.5–1.1	0.8–1.3
K_2O	0.1–0.7	0.2–0.5	0.3–0.6	0.3–0.5	0.2–0.7	12.5–15.9	14.8–17.2	12.1–12.6	14.9–16.3	15.1–15.6
Total	100.6–101.8	100.5–102.1	101.5–102.0	100.4–102.1	99.9–102.1	100.2–101.1	100.7–101.3	100.9–100.1	101.1–101.8	98.4–100.7
Si	9.2–10.3	9.7–10.8	9.8–9.9	9.8–10.2	10.0–10.6	11.8–12.0	11.9	11.8	11.8–11.9	11.7–11.8
Ti	0.0	0.0	0.0	0.0	0.0	0.0–0.01	0.0	0.0–0.01	0.0	0.0–0.02
Al	5.7–6.9	5.2–6.3	5.9–6.2	5.8–6.2	5.3–6.6	4.2–4.3	4.2	4.2–4.3	4.2–4.3	4.2–4.3
Fe^{2+}	0.04–0.06	0.03–0.05	0.06–0.07	0.04–0.05	0.03–0.06	0.0–0.02	0.01	0.01–0.02	0.01	0.0
Ca	1.5–2.1	1.0–2.9	2.0	1.6–2.0	0.9–1.9	–	–	–	–	–
Mn	–	–	–	–	–	0.0	0.0	0.0	0.0	0.0–0.01
Na	1.7–2.3	1.8–3.1	2.0–2.4	1.9–2.4	1.8–3.1	0.3–0.9	0.4–0.5	1.0–1.1	0.2–0.4	0.4–0.5
K	0.0–0.2	0.1	0.1–0.2	0.0–0.10	0.1–0.2	2.9–3.7	3.4–3.5	2.8–2.9	3.5–3.8	3.6–3.7
Or	0.9–3.7	1.1–3.0	1.6–3.1	1.6–2.6	1.4–4.3	74.0–93.7	87.0–89.4	71.5–73.3	90.6–95.7	88.4–93.0
Ab	43.8–58.2	46.0–75.4	49.5–52.3	48.0–58.4	50.8–72.0	6.4–24.2	10.7–13.1	26.2–27.6	4.3–9.4	7.0–11.6
An	38.2–52.9	23.2–52.3	44.6–48.9	39.6–49.4	26.6–45.7	0.0–1.8	0.0	0.5–0.8	0.0–0.05	0.0

Structural formula on the basis of 32 oxygen atoms

n sample number, *min* minimum values, *max* maximum values, *Qtz* Quartz, *Hbl (hbl)* Hornblende, *Bt (bt)* Biotite

Table 3 Microprobe analysis of hornblende, biotite and pyroxene from the Torul pluton

Rock types	Hornblende					Rock types	Biotite					Rock types	Pyroxene	
	Gd (n = 5)	Bt-hbl-mg (n = 5)	Qtz-mnzd (n = 3)	Qtz-mnz (n = 3)	Hbl-bt-mg (n = 5)		Gd (n = 3)	Bt-hbl-mg (n = 3)	Qtz-mnzd (n = 3)	Qtz-mnz (n = 3)	Hbl-bt-mg (n = 3)		Qtz-mnz (n = 3)	Hbl-bt-mg (n = 3)
SiO_2	49.8–53.7	48.0–53.4	49.5–49.9	50.4–52.7	47.8–52.9	SiO_2	36.2–38.4	35.9–37.3	36.8	36.5–37.3	36.6–37.3	SiO_2	50.5–52.2	50.5–53.6
TiO_2	0.1–0.7	0.5–1.3	0.9–1.1	0.4–0.6	0.1–1.1	TiO_2	4.3–6.1	5.2–5.4	5.7	4.7–5.5	5.1–5.6	TiO_2	0.6–0.9	0.1–0.6
Al_2O_3	2.1–4.9	1.8–6.1	4.6–5.0	2.2–3.6	3.0–5.9	Al_2O_3	13.1–13.6	14.1–14.9	14.2	13.8–14.3	14.2	Al_2O_3	3.1–4.5	0.6–3.6
Cr_2O_3	0.0–0.1	0.0–0.1	0.0	0.1	0.0–0.1	Cr_2O_3	0.0–0.1	0.0–0.1	0.1	0.1	0.1	Cr_2O_3	0.0	0.0
FeO	8.1–13.4	10.3–14.8	13.4–13.7	13.9–14.3	13.4–14.4	FeO	17.2–18.0	13.8–19.3	14.2	16.4–18.6	16.8–18.1	FeO	12.6–13.7	6.7–13.6
MnO	0.3–0.7	0.3–1.1	0.6–0.7	0.5–0.8	0.5–0.8	MnO	0.3	0.3–0.5	0.2	0.2–0.3	0.3–0.4	MnO	0.1	0.4–0.6
MgO	15.1–19.2	14.1–17.3	16.4–16.5	15.1–15.9	14.0–16.1	MgO	13.0–13.8	12.0–15. 7	15.2	13.0–14.1	13.0–13.4	MgO	15.2–15.7	15.1–15.8
CaO	11.3–12.6	11.3–12.0	11.0–11.6	10.7–12.1	10.4–12.8	CaO	0.0–0.1	0.1	0.1	0.0	0.1	CaO	11.8–12.9	11.5–24.3
Na_2O	0.3–1.1	0.8–1.6	1.2–1.3	0.6–0.9	0.4–1.7	Na_2O	0.1–0.2	0.2	0.3	0.1–0.2	0.1	Na_2O	0.7–0.8	0.2–0.8
K_2O	0.1–0.4	0.2–0.7	0.4–0.5	0.2–0.3	0.1–0.6	K_2O	9.2–9.3	9.0–9.5	8.7	8.9–9.8	9.3	K_2O	0.2–0.3	0.0–0.3
Total	96.9–98.1	97.4–98.3	97.7–98.8	96.6–98.6	96.7–98.1	Total	94.5–96.8	96.5–97.4	95.4	96.4–97.7	96.4–97.6	Total	98.2–98.7	97.2–101.2
TSi	7.3–7.6	7.0–7.7	7.0–7.1	7.3–7.5	7.0–7.5	Si	5.7–6.0	5.7–5.8	5.7	5.7–5.8	5.7–5.8	TSi	1.9–2.0	1.9–2.0
TAl	0.3–0.8	0.3–1.0	0.7–0.8	0.4–0.6	0.5–0.9	Ti	0.5–0.7	0.6	0.7	0.6	0.6–0.7	TAl	0.0–0.1	0.0–0.1
Tfe^3	0.0–0.1	0.0–0.1	0.1–0.2	0.0–0.1	0.0–0.1	Al	2. 5	2.6–2.8	2.6	2.5–2.6	2.6	Tfe^3	0.0	0.0
CAl	0.0	0.0–0.1	0.0–0.1	0.0	0.0–0.3	Cr	0.0	0.0	0.0	0.0	0.01	M1Al	0.1	0.0–0.1
CCr	0.0	0.0	0.0	0.0	0.0	Fe^{2+}	2.2–2.4	1.8–2.5	1.9	2.1–2.4	2.2–2.3	M1Ti	0.0	0.0
Cfe^3	0.3–0.4	0.2–0.4	0.6–0.7	0.3–0.6	0.4–0.6	Mn	0.0	0.0–0.1	0.0	0.0–0.1	0.0–0.1	$M1Fe^3$	0.0	0.0–0.1
CTi	0.0–0.1	0.0–0.1	0.1	0.0–0.1	0.0–0.1	Mg	3.1–3.2	2.8–3.6	3.5	3.0–3.3	3.0–3.1	$M1Fe^2$	0.0	0.0–0.1
CMg	3.3–4.0	3.1–3.7	3.5	3.3–3.4	3.0–3.4	Ca	0.0	0.0	0.0	0.0	0.0	M1Mg	0.9	0.8–0.9
Cfe^2	0.6–1.1	0.9–1.5	0.7–0.8	0.9–1.3	0.9–1.3	Na	0.0–0.1	0.1	0.1	0.0–0.1	0.0	M2Mg	0.0	0.0
CMn	0.0–0.1	0.0–0.1	0.0–0.1	0.0–0.1	0.0–0.1	K	1.8–1.9	1.8–1.9	1.7	1.8–1.9	1.9	$M2Fe^2$	0.4	0.0–0.4
Bfe^2	0.0–0.1	0.0–0.1	0.1	0.0–0.1	0.0–0.1	Al^6	0.2–0.4	0.3–0.4	0.3	0.3	0.3–0.4	M2Mn	0.0	0.0
BMn	0.0–0.1	0.0–0.1	0.0–0.1	0.0–0.1	0.0–0.1	Al^4	2.0–2.3	2.3–2.4	2.3	2.2–2.3	2.2–2.3	M2Ca	0.5	0.5–1.0
BCa	1.8–1.9	1.8–1.9	1.7–1.8	1.7–1.9	1.7–2.0	Mg#	0.6	0.5–0.7	0.7	0.6	0.6	M2Na	0.1	0.0–0.1
BNa	0.0–0.1	0.1	0.1–0.2	0.1	0.0–0.2	Fe^{2+}/Fe^{2+} + Mg	0.4–0.4	0.3–0.5	0.3	0.4	0.4	M2K	0.0	0.0
ACa	0.0–2.0	0.0	0.0	0.0	0.0	Structural formula on the basis of 24 oxygen						Wo	26.4–29.1	25.8–47.4
ANa	0.1–0.2	0.1–0.3	0.2	0.1–0.2	0.1–0.3							En	47.8–48.7	41.5–49.3
AK	0.0–0.1	0.0–0.1	0.1	0.0–0.1	0.0–0.1							Fs	23.2–24.9	10.9–24.9
Mg#	0.7–0.8	0.7–0.8	0.8	0.7–0.8	0.7–0.8							Structural formula on the basis of 6 oxygen		
Structural formula on the basis of 23 oxygen														

n sample number, *min* minimum values, *max* maximum values, *Qtz* Quartz, *Hbl (hbl)* Hornblende, *Bt (bt)* Biotite, *Gd* Granodiorite, *mg* Monzogranite, *mnzd* Monzodiorite, *mnz* Monzonite

sample powders were digested in 52% HF for 4 days at 140°C on a hot plate. Rb-Sr and Sm–Nd whole-rock samples as well as Rb–Sr biotite samples were spiked with mixed ^{149}Sm–^{150}Nd and $^{87}Rb/^{84}Sr$ tracer solutions. Digested samples were dried and redissolved in 6N HCl, dried again and redissolved in 2.5N HCl. After digestion, Rb, Sr and the light rare earth elements were isolated by conventional ion exchange chromatography with a 5 ml resin bed of Bio Rad AG 50W–X12, 200–400 mesh. Sm and Nd was separated from other rare-earth elements on quartz columns using 1.7 ml Teflon powder coated with HDEHP as cation exchange medium. All isotopic measurements were made by Thermal Ionization Mass Spectrometry, on a Finnigan MAT 262 mass spectrometer in static mode. The $^{87}Sr/^{86}Sr$ and $^{143}Nd/^{144}Nd$ isotope ratios were normalized to $^{86}Sr/^{88}Sr = 0.1194$ and to $^{146}Nd/^{144}$ Nd = 0.7219, respectively. The LaJolla Nd standard gave a $^{143}Nd/^{144}$ Nd ratio of 0.511867 ± 0.000018 (2σ standard deviation, reference value 0.511850). The NBS 987 Sr standard yielded an $^{87}Sr/^{86}$ Sr ratio of 0.710266 ± 0.000020 (2σstandard deviation, reference value 0.710240). Total procedural blanks (chemistry and loading) were <200 pg for Sr and <80 pg for Nd. $^{143}Nd/^{144}Nd$ ratios are quoted in the εNd notation as deviations from a chondritic reference (CHUR) with present-day $^{143}Nd/^{144}Nd$ ratio of 0.512638. Based on external reproducibility of ten separate standard loads of granite G2 (USGS standard material), uncertainties of 1.5% for $^{87}Rb/^{86}$ Sr ratio and 0.05% for the $^{87}Sr/^{86}Sr$ (2σ confidence level) were used for biotite age calculation. The uncertainty of the initial isotope ratio resulting from age correction varies between 0.02 and 0.03% (for formulae see Siebel et al. 2005).

Oxygen was extracted from approximately 10 mg of dried whole-rock powder using modified versions of the standard techniques of the flow scheme silicate line (Clayton and Mayeda 1963) at 600°C by employing BrF_5 as reagent. Quantitative oxygen yields were between 95 and 100%. Oxygen was converted to CO_2 at a graphite rod heated by a Pt-coil and CO_2 was analysed for its $^{18}O/^{16}O$ ratio with a Finnigan MAT 251 gas source mass spectrometer at the University of Tübingen. The isotopic ratios are reported in the δ-notation relative to Vienna standard mean ocean water (V-SMOW). All analyses were duplicated and analytical precision is better than ±0.2‰. A $\delta^{18}O$ value of +9.7 ± 0.1‰ ($1\sigma_m$) was obtained for the NBS–28 quartz standard and all data are normalized to this value.

Results

Petrography and field relations

Petrographic characteristics of the Torul granitoids are presented in Table 1. The QAP (quartz–alkali feldspar–plagioclase) modal classification (Streckeisen 1976) is used here to address the rock types in Torul pluton (Fig. 3).

Syenogranites are the oldest rocks, and form two circular intrusions near the centre of the pluton in areas with smooth surfaces where the relief has been largely eroded away. Granodiorites and biotite hornblende monzogranites constitute the bulk of the pluton (Fig. 2). The granodiorites are grey to light grey in colour and have a fine to medium-grained texture, which is feldspar porphyritic near the contact to the country rocks. Contacts between the gran-

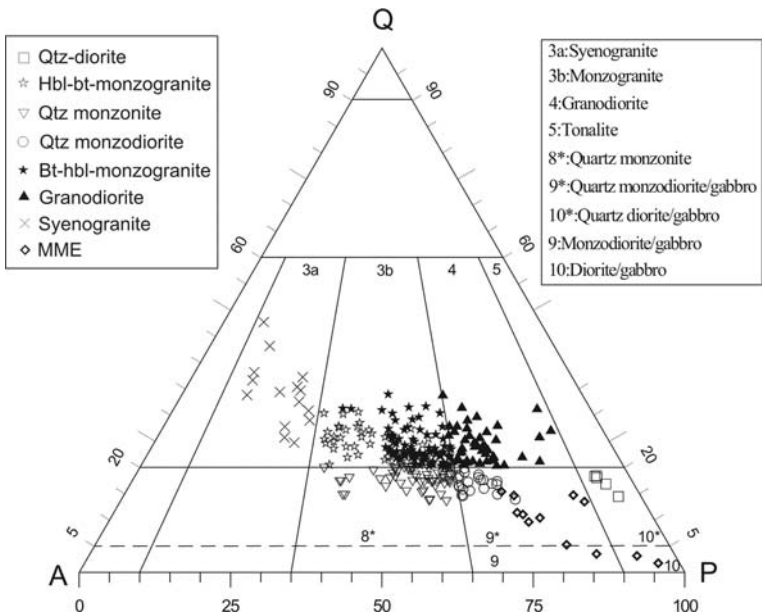

Fig. 3 Classification based on modal compositions of the Torul granitoid (Streckeisen 1976)

odiorites and the biotite hornblende monzogranites are gradational. The biotite hornblende monzogranites are medium-grained and pink to pinkish grey in colour. The quartz monzodiorites, quartz monzonites and biotite hornblende monzogranites occur within the centre of the elliptically shaped pluton (Fig. 2). Internal contacts between all these intrusions are gradational but the quartz monzodiorites and quartz monzonites have sharp contacts with the granodiorites and biotite–hornblende monzogranites. The quartz monzodiorites are medium-grained and grey to dark grey in colour. The quartz monzonites are grey to light grey in colour and medium-grained but grain size decreases towards the contacts. The hornblende biotite monzogranites are fine to medium-grained and hypidiomorphic to porphyritic with feldspar crystals, and pink to pinkish grey in colour. The young quartz diorites comprise dark green to dark grey rocks forming small outcrops at the northern and southern central margin of the pluton where they intrude the granodiorites and biotite hornblende monzogranites (Fig. 2). Contacts between the quartz diorites and these rocks are sharp. The quartz monzodiorites, granodiorites and monzogranites also contain mafic microgranular enclaves (MMEs). The contacts between the enclaves and the host rocks are sharp.

Rock samples are generally holocrystalline, fine to medium grained, porphyric, poikilitic, myrmekitic, anti-rapakivi and rarely micrographic (Fig. 4a) in texture. Towards the contact with the volcanic country rocks, the granitoids possess fine-grained textures; towards the centre of the pluton medium-grained textures predominate. Porphyric textures are generally seen close to the contact of the volcanic country rocks, especially in the quartz diorites, rarely in the syenogranites and in the contact zones of the different rock types. Plagioclase, K-feldspar, quartz, hornblende, biotite, pyroxene and actinolite-tremolite are major mineral phases in all rock types; titanite, allanite, apatite, zircon, epidote and opaque minerals form accessory minerals; secondary minerals comprise chlorite, calcite, sericite and clay minerals.

Plagioclase mainly forms subhedral to anhedral, normally and reversely zoned prismatic and lath-shaped crystals. Grain size variations range from 0.2 mm for inclusions to 2.5 mm for large crystals. A wide range in anorthite composition (An_{23} to An_{53}, Table 2) can be found. The anorthite component decreases from rim to centre of the intrusion. Plagioclase mainly shows oscillatory zoning (Fig. 4b), albite twinning and prismatic-cellular growth. Normally zoned plagioclase has ~An_{46} in the centre and ~An_{26} at the rim. A myrmekitic texture is observed at the grain boundaries between orthoclase and plagioclase. Plagioclase also shows anti-rapakivi texture, mantled by orthoclase. Some plagioclase crystals have poikilitic textures, in which large plagioclase crystals (up to 2.5 mm) may contain small crystals of plagioclase (Fig. 4c), hornblende, biotite and apatite. Some large plagioclase crystals are altered to sericite and clay minerals.

K-feldspar forms anhedral, rarely subhedral crystals of perthitic orthoclase. Large phenocrysts (up to 3 mm) are heterogeneously distributed within the various rock types (Fig. 4d). K-feldspar composition is characterized by a variation in orthoclase content ranging from Or_{72} to Or_{95} (Table 2). The mineral shows a poikilitic texture in which abundant quartz, biotite, hornblende, plagioclase and opaque minerals are included in large K-feldspar oikocrysts (Fig. 4e). Alteration to clay minerals is more common in large K-feldspar crystals than in plagioclase.

Quartz is anhedral in shape and fills interstices between other minerals. It generally shows undulose extinction and its grain size becomes increasingly smaller in the contact zones between the different rock types.

Hornblende occurs as small euhedral to subhedral tabletish prismatic crystals. Its composition varies from Mg-hornblende through actinolitic hornblende to actinolite. Mg-number (Mg# = atomic ratios Mg/(Mg + Fe), where Fe is total iron) varies between 0.7 and 0.8 (Table 3). Hornblende is abundant in the quartz diorites and granodiorites. Towards the contact with the country rocks and in the transition zones between the different intrusions, the mineral is altered into chlorite, calcite and actinolite. In the quartz diorites, actinolitic hornblende and actinolite occur, whereas magnesium-hornblende is found mainly in the centres of the other intrusions. Large hornblende crystals (2–2.5 mm) may contain small plagioclase and biotite inclusions (Fig. 4f).

Biotite is abundant in the monzogranites and syenogranites. It is euhedral and subhedral reddish-brown and forms prismatic crystals and lamellas. In some samples, especially in those from the contact zones, biotite is altered into chlorite, epidote and opaque mineral along the cleavage planes. Biotite is Mg-rich ($Fe^{2+}/Fe^{2+} + Mg =$ 0.3–0.5, Table 3), and some large crystals (2–2.5 mm) may contain small plagioclase and opaque minerals showing poikilitic texture (Fig. 4g).

Pyroxene forms subhedral to anhedral crystals and is found less frequently than the other mafic minerals. Its composition is mainly augite and rare diopside. It is characterized by varying wollastonite content, ranging from 26 to 47% (Table 3). Some minerals are altered into uralite and calcite.

Titanite forms euhedral and subhedral crystals in all rock types but was not observed in the quartz diorites. Allanite occurs as euhedral, reddish crystals in all rock types except the granodiorites and quartz diorites. Needle-like crystals of apatite are mainly found in plagioclase. Zircon is seen as short euhedral and prismatic crystals within all rock types except the quartz diorites.

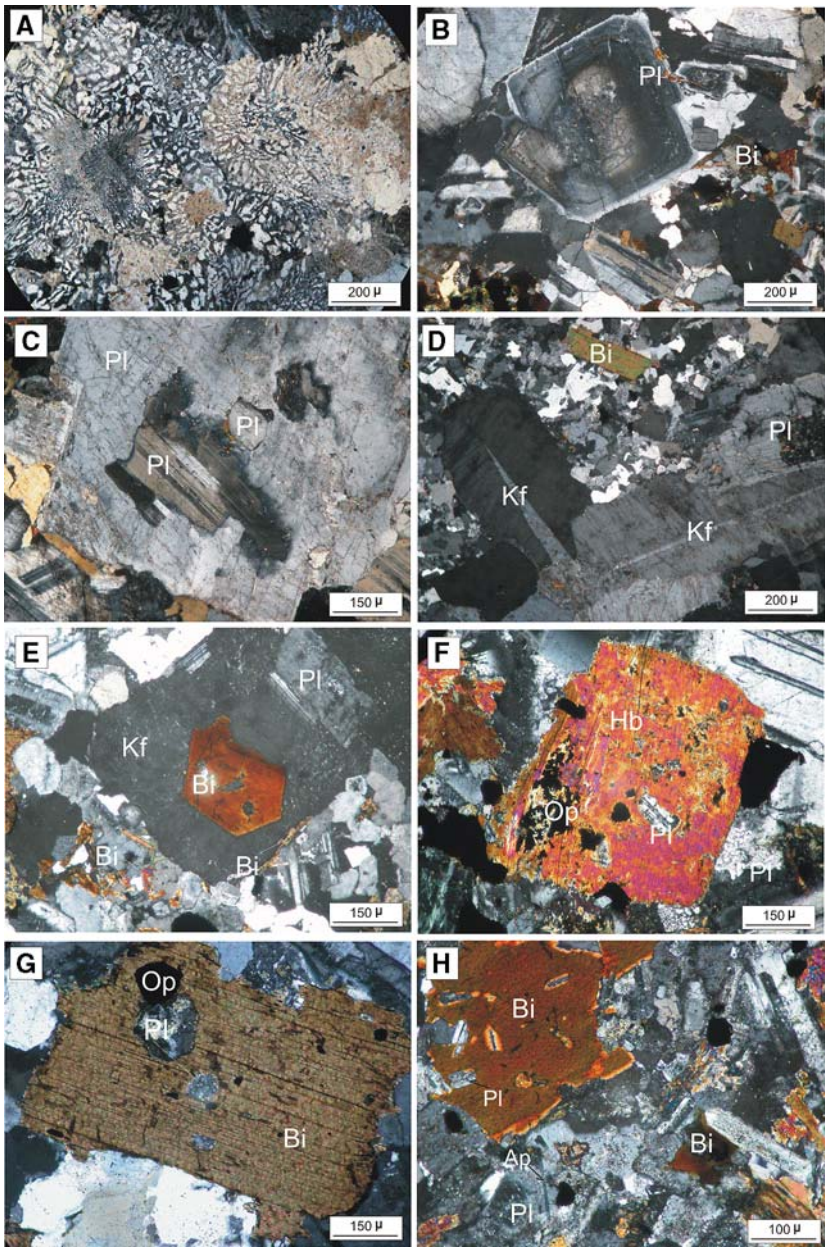

Fig. 4 **a–h** Microphotographs showing certain textural features of the Torul granitoids and associated rocks: **a** graphic texture; **b** oscillatory zoning in the plagioclase; **c** poikilitic texture in plagioclase in which some large plagioclase may contain small plagioclase crystals; **d** K-feldspar megacrystals; **e** biotite, plagioclase and opaque mineral inclusions in large K-feldspar; **f** plagioclase and opaque mineral inclusions in large hornblende crystals; **g** small plagioclase and hornblende in large biotite crystals; **h** accicular apatite crystals in the plagioclase, and poikilitic biotite with fine-grained plagioclase in MMEs (*Pl* Plagioclase, *Kf* K-feldspar, *Bi* Biotite, *Hb* Hornblende, *Q* Quartz, *Ap* Apatite, *Op* Opaque minerals)

The MMEs of different sizes (0.5 to 9 cm) are ubiquitous in the Torul pluton. The MMEs are semi-rounded to ovoid in shape and very fine-grained compared to the host rock. They have quartz monzodiorite, monzodiorite and diorite compositions. MMEs have similar textural and mineralogical features as their host rocks. They consist of plagioclase, K-feldspar, quartz, hornblende, biotite, pyroxene, accompanied by accessory apatite, zircon and opaque minerals (magnetite). Plagioclase is subhedral, andesine (An_{42-49}, optically) in composition, and has oscillatory zoning and albite-law twinning. Hornblende is the most abundant mafic mineral. Biotite is abundant at contacts between enclave and host rock, and may show chloritization. Acicular apatite, 0.2 mm in maximum length, is a frequent mineral in most MMEs (Fig. 4h). Such crystals are described from mafic melt globules trapped in silicic magmas and often cited as evidence of quenching (Wyllie et al. 1962).

Major and trace elements

Chemical analyses of representative samples from the Torul pluton are given in Tables 4 and 5. In the diagram of Debon and Le Fort (1982), the samples plot in quartz diorite/gabbro, granodiorite, quartz monzodiorite, quartz monzonite, adamellite and granite fields (Fig. 5), consistent with the QAP classification (Fig. 3). The term ''adamellite'' is obsolete and monzogranite is used instead

Table 4 Whole-rock major (wt%) and trace (ppm) element analyses of representative samples and CIPW norms of the granitoids from the Torul pluton

Sample	Syenogranite			Granodiorite						Biotite hornblende monzogranite					Quartz monzodiorite					
	T 637	63	348	T 332	T-470	T-416	T-388	T-495	T 686	356	z 79 b	T 110	66	T-449	115	85	15	191	167	343
SiO_2	69.60	71.32	73.48	60.11	61.47	62.31	63.16	63.75	64.72	63.32	64.08	66.20	67.45	68.22	57.27	58.79	59.63	60.02	60.64	61.00
TiO_2	0.36	0.34	0.29	0.73	0.69	0.60	0.55	0.50	0.49	0.53	0.45	0.38	0.37	0.30	0.68	0.60	0.59	0.58	0.55	0.50
Al_2O_3	14.35	14.28	14.18	16.39	15.03	14.97	14.90	14.95	16.28	15.70	16.55	15.85	15.86	15.04	17.14	17.05	16.66	16.56	16.37	16.26
$Fe_2O_3^T$	3.87	3.47	2.15	7.26	7.14	7.07	6.79	5.71	5.52	6.30	4.55	4.89	4.36	3.60	9.76	7.27	8.32	7.97	7.03	5.89
MnO	0.04	0.05	0.03	0.12	0.10	0.08	0.10	0.08	0.05	0.08	0.06	a.l.a	0.10	0.07	0.15	0.11	0.11	0.09	0.08	0.05
MgO	1.28	0.56	0.41	3.83	3.63	2.75	2.65	2.34	2.02	1.60	1.97	1.72	1.38	0.77	3.05	2.27	2.88	2.83	1.92	1.54
CaO	1.58	1.37	1.16	6.48	5.45	4.78	4.40	3.99	4.31	3.82	3.38	2.93	2.36	1.89	5.18	5.08	5.06	4.73	4.50	4.32
Na_2O	3.21	3.44	3.79	2.84	2.93	3.16	3.05	3.35	3.64	3.42	3.42	3.35	3.50	3.36	3.11	3.33	3.16	3.12	3.46	3.67
K_2O	5.08	5.17	5.42	2.38	2.98	3.39	3.70	3.66	3.85	3.81	4.09	4.42	4.22	4.48	3.31	3.43	3.42	3.51	3.56	3.65
P_2O_5	0.07	0.07	0.06	0.19	0.18	0.17	0.15	0.16	0.15	0.16	0.13	0.14	0.14	0.12	0.19	0.18	0.15	0.17	0.17	0.17
LOI	0.22	0.25	0.12	0.45	0.37	0.27	0.38	0.64	0.42	0.68	0.72	0.62	0.73	0.97	0.68	0.96	0.44	0.37	0.78	0.97
Total	99.66	100.3	101.1	100.8	99.97	99.55	99.83	99.13	101.5	99.42	99.40	100.5	100.5	98.82	100.5	99.07	100.4	99.95	99.06	98.02
Cr	NA	6	5	NA	46	26	NA	17	NA	47	NA	NA	18	3	54	49	NA	60	46	24
Ni	NA	2	1	12	5	6	11	4	NA	4	2	3	5	3	7	3	5	3	5	5
Pb	NA	81	51	20	65	44	19	64	NA	68	17	27	168	51	95	175	66	177	59	80
Rb	224	246	259	68	91	105	119	136	131	134	126	140	159	164	103	120	118	124	120	126
Ba	1137	1242	1352	853	915	1130	1197	1109	1198	1046	1064	1167	1352	1441	1030	1243	1015	1046	1217	1329
Sr	158	127	106	352	340	329	339	328	326	294	266	263	258	254	350	343	337	325	340	329
Nb	16	16	18	7	14	10	11	10	NA	11	12	19	14	17	5	6	12	13	9	11
Zr	152	201	211	115	127	161	118	166	160	166	184	162	176	196	140	159	146	154	155	154
Ta	1.1	NA	1.15	0.5	NA	NA	1.24	NA	0.6	NA	0.79	1.25	NA	NA	1.1	NA	1.2	NA	1.42	NA
Y	26	28	34	16	15	14	16	18	19	15	18	17	21	24	12	13	11	14	15	14
Th	44	47	46	24	22	26	19	28	31	33	36	35	33	41	17	15	24	37	27	33
Hf	3.85	NA	3.92	1.02	NA	NA	1.3	NA	2.86	NA	1.83	3.25	NA	NA	NA	NA	1.44	NA	1.62	NA
U	8.2	NA	8.6	3.36	NA	NA	2.99	NA	4.1	NA	4.53	6.9	NA	NA	NA	NA	2.27	NA	NA	NA
Q	26.53	27.93	27.50	16.63	17.96	18.50	19.44	19.78	17.60	19.33	18.94	21.34	24.26	27.24	11.71	13.33	14.08	14.95	15.69	15.77
Or	30.22	30.56	31.75	14.03	17.70	20.20	22.01	21.98	22.54	22.82	24.52	26.18	25.03	27.08	19.61	20.68	20.23	20.85	21.43	22.25
Ab	27.28	29.05	31.72	23.92	24.86	26.90	25.92	28.75	30.45	29.27	29.29	28.35	29.66	29.02	26.33	28.69	26.71	26.48	29.75	31.96
An	7.47	6.39	5.35	24.82	19.09	16.73	16.08	15.13	16.49	16.39	16.23	13.74	10.92	8.87	23.02	21.81	21.13	20.85	18.90	17.58
C	0.83	0.67	0.08	0.00	0.00	0.00	0.00	0.00	0.00	0.00	0.62	0.51	1.53	1.50	0.00	0.00	0.00	0.00	0.00	0.00
Di wo	0.00	0.00	0.00	2.56	2.93	2.57	2.09	1.68	1.59	0.78	0.00	0.00	0.00	0.00	0.68	1.18	1.30	0.72	1.17	1.45
Di en	0.00	0.00	0.00	2.21	2.52	2.22	1.80	1.45	1.37	0.67	0.00	0.00	0.00	0.00	0.58	1.01	1.12	0.62	1.01	1.25
Hy en	3.22	1.40	1.02	7.34	6.59	4.71	4.86	4.49	3.63	3.38	4.99	4.31	3.46	1.97	7.05	4.77	6.08	6.48	3.87	2.71
Mt	0.13	0.16	0.10	0.39	0.33	0.26	0.33	0.27	0.16	0.26	0.20	0.00	0.33	0.23	0.49	0.37	0.36	0.30	0.27	0.17
He	3.80	3.35	2.06	6.97	6.94	6.94	6.60	5.61	5.35	6.20	4.47	4.90	4.15	3.52	9.44	7.16	8.07	7.80	6.97	5.95
Ap	0.15	0.15	0.13	0.41	0.39	0.37	0.33	0.35	0.32	0.35	0.29	0.31	0.31	0.27	0.42	0.40	0.33	0.37	0.38	0.38
Mg#	24.85	13.90	16.02	34.54	33.70	28.00	28.07	29.07	26.79	20.25	30.21	26.02	24.04	17.62	23.81	23.79	25.72	26.20	21.45	20.73
ASI	1.05	1.04	1.00	0.86	0.84	0.85	0.88	0.89	0.90	0.94	1.02	1.01	1.09	1.09	0.95	0.93	0.92	0.94	0.92	0.91

Table 4 continued

Sample	Quartz mnzdy		Quartz monzonite					Hornblende biotite monzogranite					Quartz diorite			MME				
	T 647	T 608	326	245	83	79	T-401	T 446	T 432	127	T 658	T-455	T 59	T 58	T57	T500	728	608	12	438
SiO_2	61.67	62.48	58.26	59.67	60.09	60.62	61.78	61.75	62.23	63.73	64.26	64.78	52.22	53.16	54.98	53.39	53.46	53.69	55.85	56.74
TiO_2	0.48	0.53	0.64	0.63	0.54	0.53	0.50	0.53	0.52	0.48	0.52	0.44	0.94	0.88	0.85	0.92	0.76	0.83	0.81	0.81
Al_2O_3	16.28	16.34	16.51	16.22	16.32	16.33	15.88	16.08	16.61	16.05	15.61	14.91	19.86	19.12	18.86	17.98	17.75	16.79	17.08	17.07
$Fe_2O_3^T$	6.71	5.48	8.01	8.10	6.77	7.40	7.09	6.35	5.05	5.01	5.32	5.00	9.39	8.85	8.25	8.02	8.78	9.07	9.11	7.72
MnO	0.07	0.07	0.10	0.10	0.09	0.10	0.08	0.10	0.08	0.06	0.06	0.07	0.14	0.12	0.11	0.13	0.14	0.08	0.09	0.11
MgO	2.47	1.56	2.88	2.76	2.22	2.02	2.22	2.54	1.76	1.51	2.02	1.92	5.64	5.02	4.85	4.21	4.02	3.94	2.89	2.73
CaO	4.73	4.35	5.08	4.76	4.71	4.13	4.37	4.12	4.10	4.05	3.12	3.58	9.55	8.92	8.12	7.76	6.65	5.17	5.39	5.21
Na_2O	3.22	3.81	3.00	3.04	2.95	3.43	3.11	2.79	3.23	3.22	3.12	3.23	2.27	2.43	2.52	4.57	3.59	4.37	3.79	4.07
K_2O	3.76	3.96	3.82	3.62	3.91	3.81	3.96	3.72	3.83	4.26	4.46	4.41	0.75	1.12	1.42	1.43	2.33	2.44	2.43	2.58
P_2O_5	0.14	0.11	0.17	0.16	0.14	0.16	0.17	0.17	0.16	0.14	0.12	0.14	0.33	0.31	0.28	0.32	0.23	0.10	0.20	0.17
LOI	0.37	0.64	0.76	0.68	0.69	0.78	0.46	0.98	0.95	0.89	0.72	0.88	0.27	0.34	0.42	0.31	2.21	2.55	2.35	1.94
Total	99.90	99.33	99.23	99.74	98.43	99.31	99.62	99.13	98.52	99.40	99.33	99.36	101.4	100.3	100.7	99.04	99.92	99.03	99.99	99.15
Cr	NA	NA	NA	51	46	45	30	NA	NA	34	NA	NA	86	82	75	NA	NA	NA	NA	NA
Ni	3	NA	4	4	2	5	2	7	6	3	NA	4	25	23	20	NA	NA	NA	NA	NA
Pb	NA	NA	58	99	109	83	49	21	18	48	NA	18	NA	NA	NA	NA	NA	NA	NA	NA
Rb	138	142	122	137	142	154	162	137	138	165	163	167	27	30	36	55	99	70	87	105
Ba	1280	1245	1249	1374	1271	1247	1345	1258	1220	1300	1305	1279	163	280	315	391	821	772	696	1223
Sr	314	308	316	297	287	279	266	316	314	269	237	222	466	452	440	389	381	373	323	343
Nb	NA	NA	12	12	11	8	11	13	12	13	NA	15	3	NA	5	NA	NA	NA	NA	NA
Zr	149	168	139	166	146	148	153	163	159	188	166	168	46	56	63	55	57	93	107	137
Ta	NA	0.82	0.71	NA	0.62	NA	NA	1.56	1.6	NA	0.8	1.76	0.18	0.2	0.22	0.70	1.00	0.30	1.80	0.70
Y	16	19	14	16	14	15	17	18	16	16	23	26	23	23	25	16	20	21	20	22
Th	NA	34	18	29	36	25	40	29	26	31	37	38	6	9	9	6.40	9.70	13.71	16.20	15.73
Hf	NA	2.23	1.45	NA	1.67	NA	NA	1.77	1.64	NA	3.23	NA	0.56	0.76	0.82	1.60	2.30	3.74	2.60	5.63
U	NA	2.9	3.49	NA	3.52	NA	3.65	2.57	2.77	NA	4.6	2.74	0.8	NA	0.9	2.10	4.20	3.00	4.00	3.00
Q	15.99	15.13	12.48	14.97	15.90	15.23	17.10	19.46	18.23	18.97	19.93	20.07	8.79	9.89	11.51	0.64	5.47	3.69	10.09	9.58
Or	22.35	23.73	22.95	21.62	23.66	22.87	23.62	22.42	23.22	25.58	26.75	26.49	4.39	6.63	8.38	6.58	14.10	14.96	14.72	15.70
Ab	27.34	32.63	25.75	25.94	25.51	29.42	26.51	24.02	27.98	27.63	26.74	27.72	18.98	20.55	21.25	29.71	31.05	38.28	32.81	35.39
An	18.90	15.95	20.56	20.06	20.14	18.13	17.77	19.82	19.90	16.96	14.99	13.31	41.28	37.93	35.82	31.88	25.98	19.64	22.91	21.24
C	0.00	0.00	0.00	0.00	0.00	0.00	0.00	0.32	0.02	0.00	0.22	0.00	0.00	0.00	0.00	0.00	0.00	0.00	0.00	0.00
Di wo	1.61	2.20	1.68	1.19	1.23	0.72	1.29	0.00	0.00	1.09	0.00	1.63	1.54	1.90	1.15	5.69	2.68	2.65	1.37	1.81
Di en	1.39	1.90	1.45	1.02	1.06	0.62	1.11	0.00	0.00	0.94	0.00	1.40	1.33	1.64	0.99	4.90	2.31	2.28	1.18	1.56
Hy en	4.81	2.05	5.86	5.94	4.62	4.50	4.48	6.47	4.51	2.89	5.12	3.47	12.62	10.92	11.50	9.40	7.98	7.92	6.22	5.46
Mt	0.23	0.23	0.33	0.33	0.30	0.33	0.26	0.33	0.27	0.20	0.20	0.23	0.45	0.39	0.36	0.51	0.47	0.27	0.30	0.37
He	6.58	5.39	7.91	7.95	6.72	7.28	6.97	6.24	4.99	4.95	5.26	4.92	8.98	8.59	7.98	8.92	8.66	9.21	9.12	7.69
Ap	0.31	0.24	0.38	0.35	0.31	0.35	0.37	0.38	0.36	0.31	0.27	0.31	0.71	0.68	0.61	0.82	0.51	0.23	0.45	0.38
Mg#	26.91	22.16	26.45	25.41	24.69	21.44	23.85	28.57	25.84	23.16	27.52	27.75	37.52	36.19	37.02	34.42	31.41	30.28	24.08	26.12
ASI	0.91	0.89	0.90	0.92	0.92	0.95	0.92	1.00	0.98	0.93	1.00	0.90	0.91	0.89	0.92	0.78	0.87	0.87	0.92	0.90

$Fe_2O_3^T$ is total iron as Fe_2O_3, Mg# (mg-number) = 100 × MgO/(MgO + $Fe_2O_3^T$), ASI = molarAl_2O_3/(CaO + Na_2O + K_2O), *LOI* loss on ignition, *NA* not analysed, *MME* mafic microgranular enclaves

Table 5 Rare earth elements analyses (ppm) of representative samples from the Torul pluton

Sample	Syenogranite		Granodiorite			Bt-hbl mg		Quartz monzodiorite			Qtz monzonite		Hbl-Bt mg			Quartz diorite		MME		
	T 637	63	T 332	T-516	T 686	z 79 b	T 110	15	T 438	T 608	326	T-401	T 446	T 432	T 658	T 59	T58	385	12	438
La	52.20	58.48	22.52	31.82	40.50	41.57	45.30	31.08	43.35	46.10	33.94	48.00	42.45	50.09	48.00	8.50	10.12	20.1	22.3	34.6
Ce	85.60	91.72	38.35	59.50	65.30	77.32	83.48	48.21	54.46	55.70	53.04	59.00	68.36	84.39	73.20	17.00	21.24	41.3	43	49.7
Pr	10.29	NA	7.19	NA	7.44	NA	NA	NA	NA	8.59	NA	NA	NA	NA	8.90	2.69	3.45	5.35	5.1	9.27
Nd	32.60	34.40	19.83	26.20	31.89	29.35	31.05	23.81	24.57	23.78	26.71	27.32	37.69	36.93	29.53	11.00	12.00	22.2	18.9	32.96
Sm	5.73	6.26	4.14	5.30	5.33	5.27	5.35	4.42	4.47	3.90	5.06	6.08	6.02	5.88	5.14	2.94	3.14	6.1	4.5	6.58
Eu	1.44	1.52	0.89	1.14	1.22	1.13	1.08	0.90	1.13	1.19	1.03	1.08	1.37	1.11	1.05	0.78	0.82	0.91	0.9	1.27
Gd	5.57	5.82	4.34	5.36	5.46	5.48	5.11	4.22	4.38	4.82	4.30	4.33	5.67	5.41	4.91	3.32	3.62	5.94	4.16	6.03
Tb	0.93	0.78	0.66	0.71	0.73	0.70	0.67	0.62	0.68	0.61	0.68	0.70	0.82	0.77	0.84	0.57	0.59	1.13	0.71	1.12
Dy	4.64	4.77	3.84	3.87	3.83	3.87	3.71	3.39	3.66	3.49	3.68	3.70	4.36	4.04	4.11	3.54	3.36	6.22	3.64	5.49
Ho	0.92	0.97	0.84	0.84	0.92	0.93	0.95	0.74	0.78	0.76	0.77	0.79	0.93	0.90	0.79	0.64	0.68	1.15	0.65	1.08
Er	2.97	2.99	2.36	2.32	2.49	2.48	2.54	2.13	2.17	2.03	2.14	2.16	2.69	2.58	2.54	2.09	2.10	3.74	2.25	3.36
Tm	0.44	0.49	0.41	0.42	0.42	0.43	0.43	0.37	0.38	0.39	0.38	0.39	0.46	0.45	0.36	0.34	0.35	0.54	0.31	0.48
Yb	3.89	3.97	2.34	2.13	2.82	2.97	3.13	2.09	2.59	2.29	2.27	2.29	3.81	3.67	3.40	2.06	2.08	3.65	1.99	3.22
Lu	0.42	0.47	0.39	0.35	0.40	0.36	0.38	0.34	0.35	0.37	0.34	0.36	0.42	0.38	0.35	0.30	0.31	0.45	0.27	0.45
$(La/Lu)_{cn}$	12.87	12.88	5.98	9.41	10.48	11.96	12.34	9.46	12.82	12.90	10.34	13.81	10.47	13.65	14.20	2.93	3.38	4.62	8.55	7.96
$(La/Sm)_{cn}$	5.73	5.88	3.42	3.78	4.78	4.96	5.33	4.43	6.10	7.44	4.22	4.97	4.44	5.36	5.88	1.82	2.03	2.07	3.12	3.31
$(Gd/Lu)_{cn}$	1.65	1.54	1.38	1.90	1.70	1.89	1.67	1.54	1.55	1.62	1.57	1.49	1.68	1.77	1.74	1.37	1.45	1.64	1.91	1.66
$(La/Yb)_{cn}$	9.07	9.95	6.50	10.09	9.70	9.46	9.78	10.05	11.31	13.60	10.10	14.16	7.53	9.22	9.54	2.79	3.29	3.72	7.57	7.26
$(Tb/Yb)_{cn}$	1.02	0.84	1.21	1.43	1.11	1.01	0.92	1.27	1.12	1.14	1.28	1.31	0.92	0.90	1.06	1.18	1.21	1.32	1.53	1.49
Eu/Eu*	0.77	0.76	0.64	0.65	0.69	0.64	0.62	0.63	0.77	0.84	0.66	0.61	0.71	0.59	0.63	0.76	0.74	0.46	0.63	0.61

*Eu** $(Sm+Gd)_{cn}$ /2, *NA* not analysed, *Qtz* Quartz, *Hbl (hbl)* Hornblende, *Bt (bt)* Biotite, *mg*: Monzogranite, *MME* Mafic microgranular enclaves

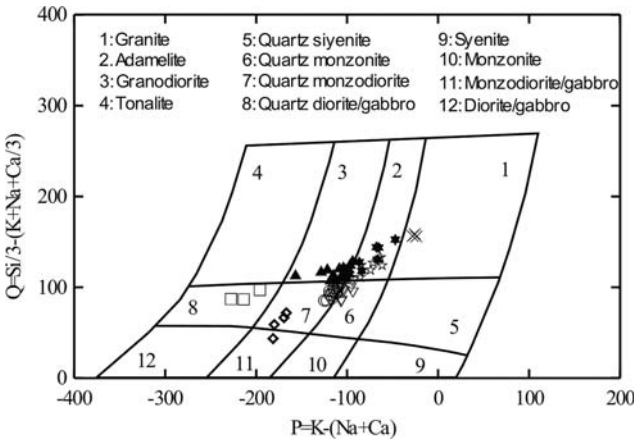

Fig. 5 Chemical nomenclature diagram (Debon and Le Fort 1982) for selected samples from the Torul pluton. See Fig. 3 for explanation

(Le Maitre et al. 1989). The MMEs plot in quartz monzodiorite and diorite/gabbro fields (Fig. 5). Quartz diorites, MMEs, the other rock types (granodiorites, biotite hornblende monzogranites, quartz monzodiorites, quartz monzonites and hornblende biotite monzogranites) and syenogranites display distinct ranges of SiO_2 contents (52–55, 53–57, 57–68 and 70–74 wt%, respectively) (Table 4; Fig. 6). Quartz diorites have lower SiO_2 content than the MMEs and the other rock types. Harker plots of selected major and trace elements (Fig. 6a–r) show systematic variation in element concentration. The aluminium saturation index, ASI [molar $Al_2O_3/(CaO + Na_2O + K_2O)$], increases with increasing SiO_2 from 0.84 to 1.09 (Fig. 6a). MMEs have similar ASI values, 0.78–0.92, as their host rocks. Apart from the quartz diorites, which belong to the medium-K series, the other rock types and the MMEs plot into the high-K field (Fig. 6b). For some major and trace elements (Fig. 6b, e, f, j, k, n, p), variation trends of the granodiorites and biotite hornblende monzogranites differ distinctly from those of the quartz monzodiorites, quartz monzonites and hornblende biotite monzogranites. Quartz diorites have the lowest K_2O, Na_2O, Rb, Th, Ba, Zr, Ce and Nb concentrations whereas syenogranites are depleted in CaO, MgO and Sr (Fig. 6b, e, f, h, k–r).

Chondrite-normalized rare earth element patterns of all rock types have concave-upward shape and are characterized by negative Eu anomalies with Eu/Eu* ranging from 0.59 to 0.84 (Fig. 7a–h; Table 5). MMEs display more negative Eu anomalies (Eu/Eu* = 0.46–0.63) than the other rock types, indicating plagioclase fractionation. The quartz diorites are less enriched in LREE compared to the other rock types and the MMEs. There is no systematic relationship between SiO_2 content and magnitude of Eu anomaly. General trends of the primitive mantle normalized element concentration diagrams are shown in Fig. 8a–h. The quartz diorites are less enriched in incompatible elements when compared to the other rock types and MMEs. All rocks show enrichment of large ion lithophile elements (LILEs), depletion of high field strength elements (HFSEs) and prominent positive Pb anomalies. The depletion in HFSEs is best expressed by negative Nb–Ta anomalies. In addition, negative P, Hf and Ti anomalies and subdued negative Y anomalies are seen in the granodiorites, biotite hornblende monzogranites, quartz monzodiorite, quartz monzonites and the hornblende biotite monzogranites (Fig. 8c–g). The quartz diorites are depleted in Hf whereas the syenogranites are characterized by depletion of P and Ti.

Rb-Sr and Sm-Nd isotopes

Rb-Sr and Sm-Nd isotopic data are listed in Table 6 and plotted in Fig. 9a–c. Rb–Sr dating of biotite minerals separated from the syenogranites gave an age of 77.9 ± 0.3 Ma. (Fig. 10) slightly older than the K-Ar age of 72.1 ± 3.6 Ma reported for a quartz monzonite sample in an earlier study (Jica 1986). Initial Sr ratios and $\varepsilon_{Nd(i)}$ values were calculated using an age of 77 Ma for all rock types. Granodiorites, biotite hornblende monzogranites, quartz monzodiorites, quartz monzonites and hornblende biotite monzogranites show a small range in Sr–Nd values (initial $^{87}Sr/^{86}Sr$ from 0.7058 to 0.7072 and $\varepsilon_{Nd(i)}$ from –3.1 to –4.1). This group comprises rocks with different chemical composition. Two out of three syenogranite samples are displaced towards lower initial $^{87}Sr/^{86}Sr$ ratios (0.7034 and 0.7042) but contain the same $\varepsilon_{Nd(i)}$ values as the other samples. The quartz diorite samples belong to the most mafic rock type of the Torul pluton, have higher initial $^{87}Sr/^{86}Sr$ ratios (0.7075 and 0.7079) and lower $\varepsilon_{Nd(i)}$ values (–4.5 and –5.3) compared to the other samples.

Oxygen isotopes

Whole-rock oxygen isotopic data are listed in Table 6 and plotted in Fig. 11a, c. $\delta^{18}O$ values of the Torul granitoids vary between +3.5 and +8.2‰, similar to those commonly found in I-type granitoids (e.g. Clarke 1992). Samples from granodiorites, biotite hornblende monzogranites, quartz monzodiorites, quartz monzonites and hornblende biotite monzogranites show an even smaller range of $\delta^{18}O$ values between +4.4 and +7.3. In the $\varepsilon_{Nd(i)}$– δ^{18} O diagram (Fig. 11a), these samples define a weak trend of slightly increasing $\delta^{18}O$ with decreasing $\varepsilon_{Nd(i)}$. A slightly positive correlation between $\delta^{18}O$ values and SiO_2 is observed for granodiorites, biotite hornblende monzogranites, quartz monzodiorites, quartz monzonites and hornblende biotite monzogranites (Fig. 11c). Such a trend, however, does not exist for the quartz diorite and syenogranite samples.

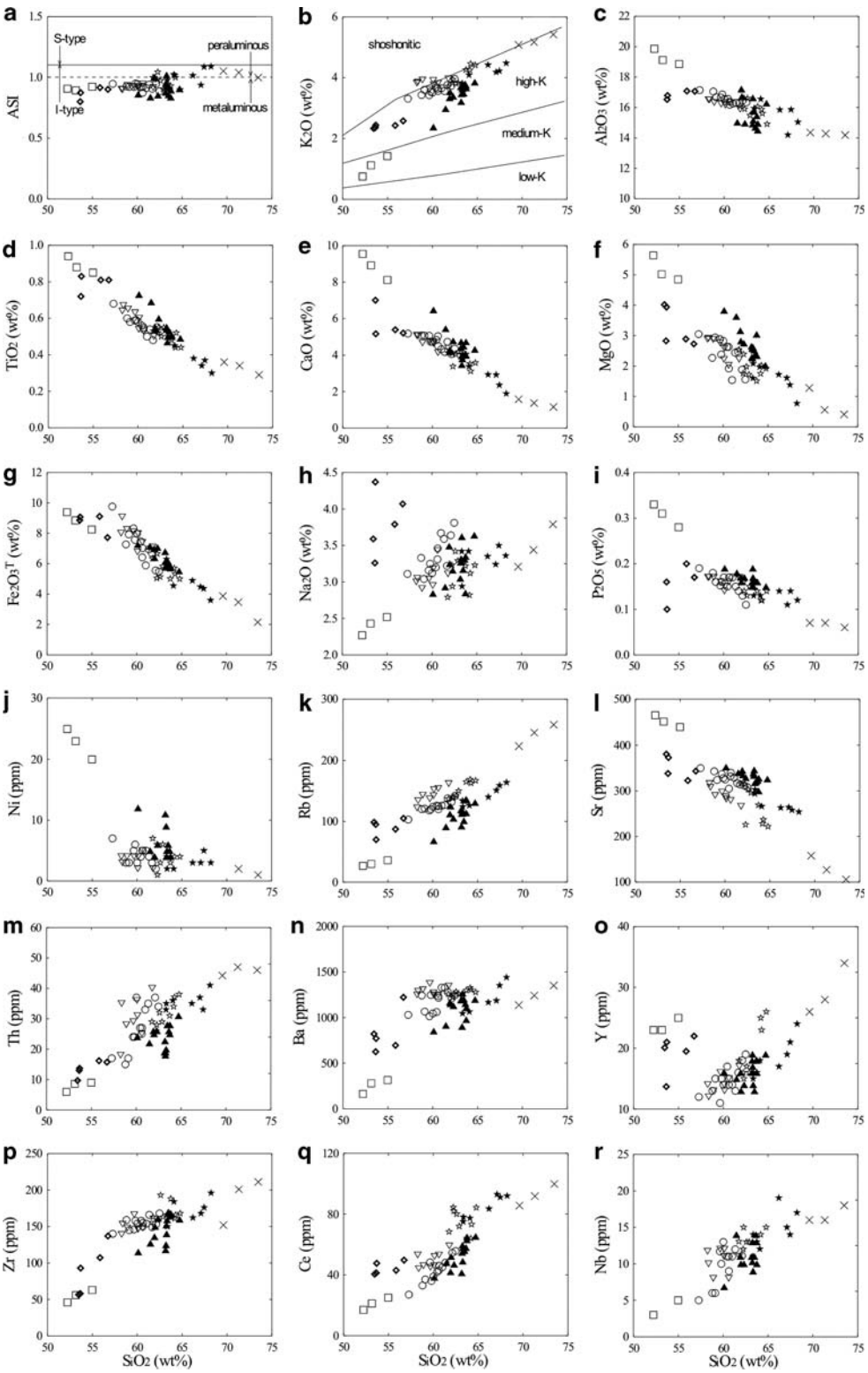

Fig. 6 **a–r** SiO_2 (wt%) versus major oxides (wt%) and trace elements (ppm) variation diagrams for samples from the Torul pluton. **a** ASI versus SiO_2 with field boundaries between I-type and S-type of Chappell and White (1974) and peraluminous and metaluminous fields of Shand (1947). **b** K_2 O versus SiO_2 diagram with field boundaries between medium-K, high-K and shoshonitic series of Peccerillo and Taylor (1976). ASI (aluminium saturation index) = molar $Al_2O_3/(Na_2$ O + K_2 O + CaO). See Fig. 3 for explanation

The measured $\delta^{18}O$ values may reflect contributions from both mantle and crustal material. Intermediate and acid crustal igneous rocks are enriched in ^{18}O relative to mantle rocks and the weak correlation between $\varepsilon_{Nd(i)}$, $\delta^{18}O$ and silica (Fig. 11) is in line with this interpretation. Some samples are lower in $\delta^{18}O$ than average mantle rocks (+5 to +6 ‰, e.g. Harmon and Hoefs 1995). Such low values can be attributed to contamination of the magmas by assimi-

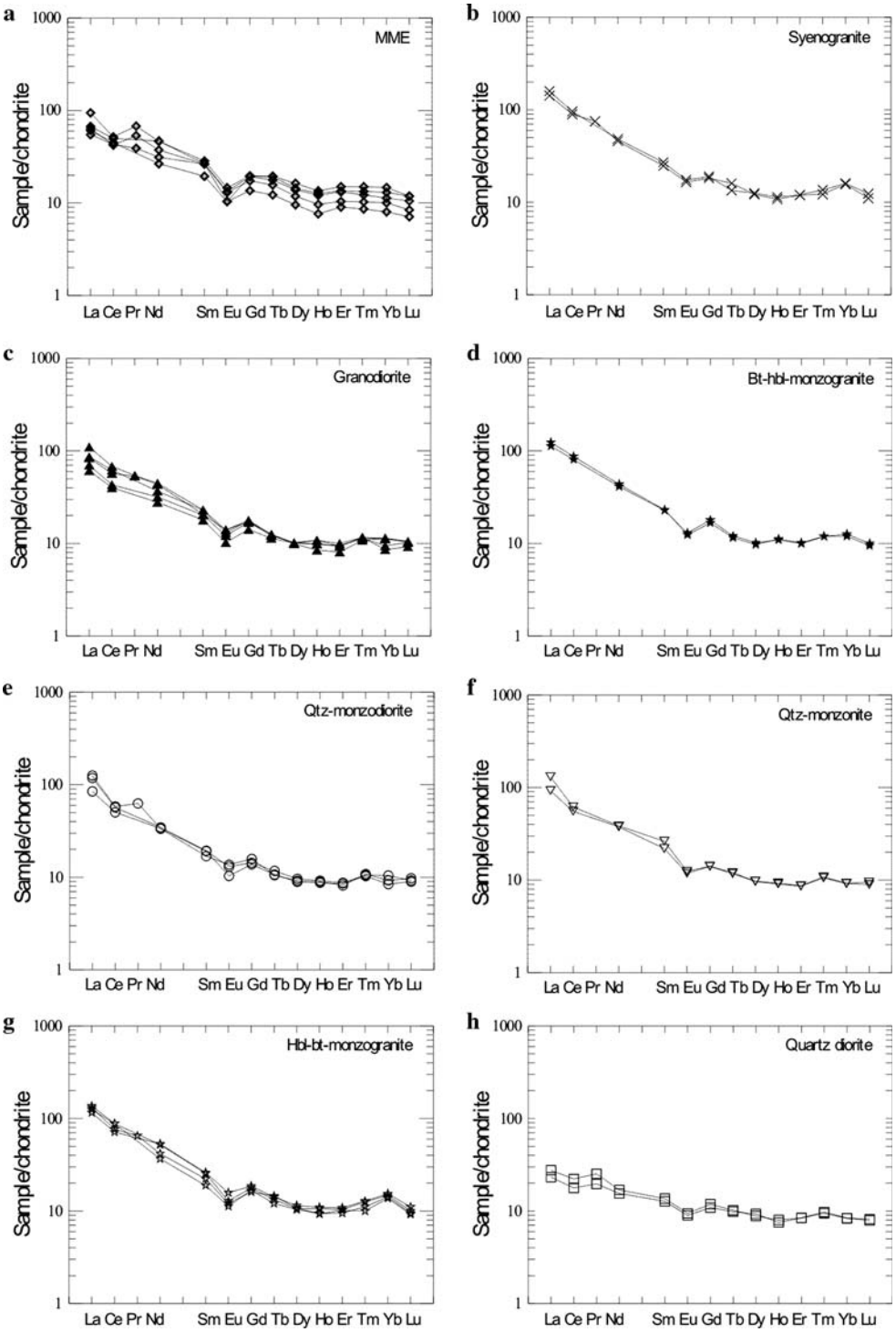

Fig. 7 **a–h** Chondrite normalized rare earth element patterns (normalizing values from Taylor and McLennan 1985) for selected samples from the Torul pluton. See Fig. 3 for explanation

lation of hydrothermally altered rocks. Alternatively, the low $\delta^{18}O$ values might be explained by hydrothermal alteration of the rocks through meteoric fluids at the subsurface. Meteoric fluids are depleted in $\delta^{18}O$ relative to silicate rocks and open-system water–rock exchange can produce a decrease in $\delta^{18}O$ in the rock phase.

Fractional crystallization

Major and trace element variation trends bear evidence that fractional crystallization has taken place during the formation of the Torul granitoids (Fig. 6). This is also supported by the depletion in Ba, Sr, P, and Eu (Fig. 8).

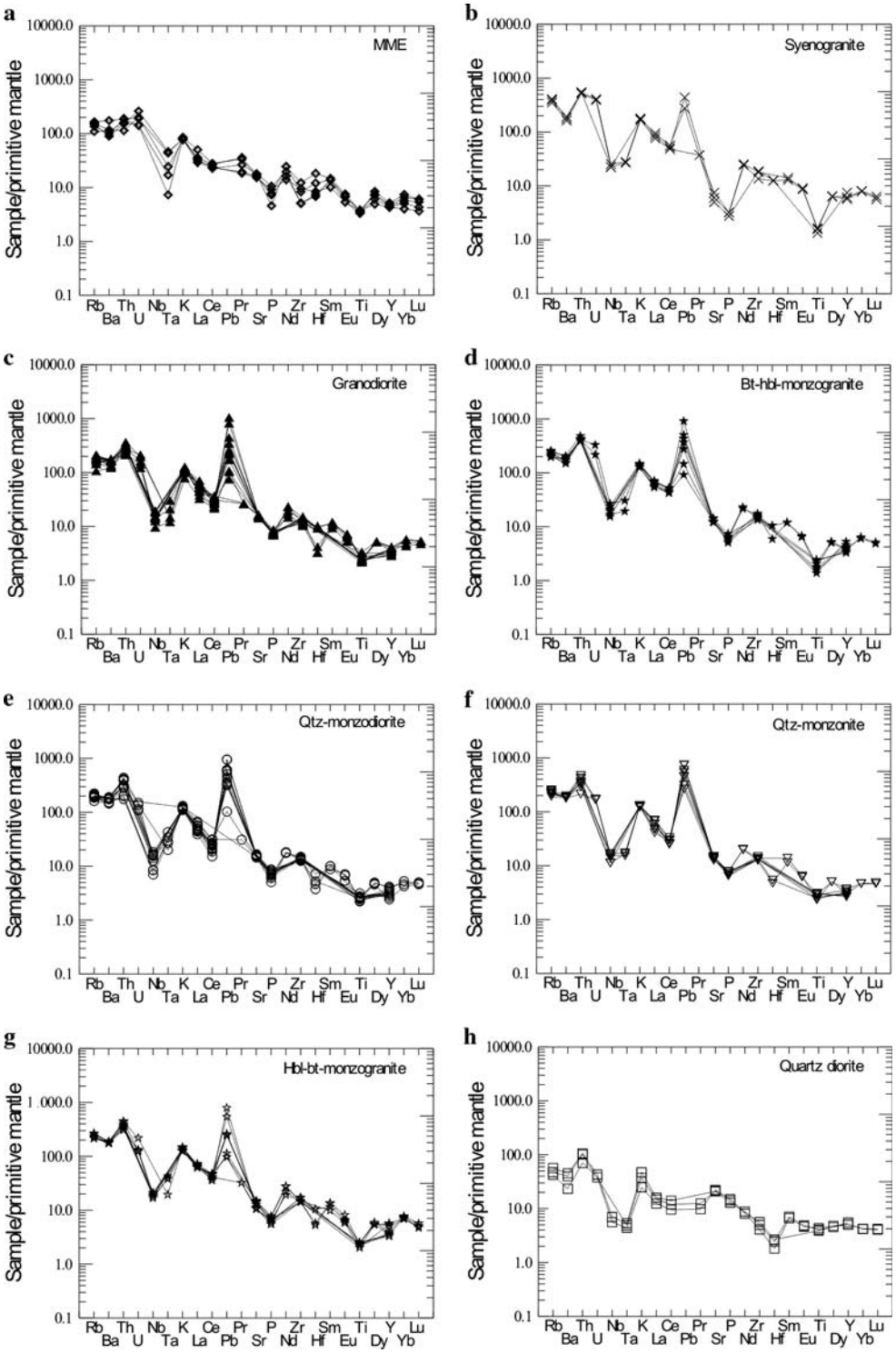

Fig. 8 a–h Primitive mantle normalized trace element patterns (normalizing values from Sun and McDonough 1989) for selected samples from Torul pluton. See Fig. 3 for explanation

Depletion in P results from removal of apatite during fractional crystallization. Negative Eu anomalies (Fig. 7) require fractionation of plagioclase and/or K-feldspar. Fractionation of feldspar would also result in depletion of Sr and Ba. Negative Eu anomalies and a decrease of Sr with increasing silica (Fig. 6 l) demonstrate that plagioclase was an important fractionating phase. The decrease of Al_2O_3, TiO_2, CaO, MgO, Fe_2O_3, P_2O_5, Sr, Ni and increase of K_2O, Rb with increasing silica (Fig. 6b–g, i–k) is related to the fractionation of plagioclase, amphibole, pyroxene, apatite and titanite. The increase of K_2O and Rb with increasing silica indicates that K-feldspar and biotite were not early fractionation phases. This is in line with the late appearance of both minerals in the crystallization sequence.

Table 6 Rb-Sr, Sm-Nd and $\delta^{18}O$ isotope data of granitoids from the Torul pluton

Sample	Sr	Rb	Sm	Nd	$^{87}Rb/^{86}Sr$	$^{87}Sr/^{86}Sr$	$(^{87}Sr^{86}Sr)_{77Ma}$	$^{147}Sm/^{144}Nd$	$^{143}Nd/^{144}Nd$	$(^{143}Nd/^{144}Nd)_{77Ma}$	εNd_{77Ma}	$\delta^{18}O$ (‰)
Syenogranite												
T637	158	224	5.18	26.8	4.102	0.707858 (10)	0.70337	0.1192	0.512393 (10)	0.512334	–4.0	7.56
348	106	259	5.41	27.3	7.072	0.711885 (10)	0.70415	0.1197	0.512406 (9)	0.512345	–3.8	4.93
63b	139	196	5.82	38.8	4.081	0.711045 (9)	0.70658	0.0911	0.512416 (9)	0.512370	–3.3	8.22
Bi 63b	6.14	534			258.6	0.992748 (12)						
Bi 63b	6.65	483			214.9	0.944178 (10)						
Granodiorite												
T470	340	91	4.64	30.5	0.774	0.707073 (10)	0.70623	0.0920	0.512425 (9)	0.512378	–3.1	4.44
11	335	125	4.95	25.3	1.080	0.707759 (9)	0.70658	0.1184	0.512403 (8)	0.512343	–3.8	6.99
T416	329	105	4.65	22.3	0.923	0.707313 (10)	0.70630	0.1261	0.512412 (7)	0.512348	–3.7	5.15
T686	326	131	5.44	30.6	1.163	0.707247 (10)	0.70598	0.1097	0.512410 (8)	0.512356	–3.6	5.45
Biotite hornblende monzogranite												
Z79	266	126	5.55	30.0	1.371	0.707974 (10)	0.70647	0.1143	0.512412 (9)	0.512355	–3.6	5.89
T110b	263	140	5.48	32.4	1.540	0.708311 (10)	0.70663	0.1043	0.512402 (9)	0.512350	–3.7	5.55
T460	264	151	3.70	19.0	1.655	0.709073 (10)	0.70726	0.1176	0.512393 (9)	0.512334	–4.0	7.29
Quartz monzodiorite												
203	328	120	4.78	24.7	1.059	0.707623 (10)	0.70647	0.1171	0.512397 (9)	0.512338	–3.9	5.79
T608	308	142	3.97	23.9	1.334	0.707218 (10)	0.70576	0.1026	0.512418 (9)	0.512367	–3.5	5.93
Quartz monzonite												
326	316	122	5.12	27.0	1.117	0.708052 (10)	0.70683	0.1168	0.512386 (9)	0.512328	–4.1	5.24
Hornblende biotite monzogranite												
T432b	314	138	5.67	33.3	1.272	0.707622 (10)	0.70623	0.1050	0.512393 (13)	0.512341	–3.9	7.04
127	269	165	5.14	26.5	1.775	0.707757 (10)	0.70582	0.1175	0.512397 (10)	0.512338	–3.9	7.31
Quartz diorite												
T59	466	27	2.76	10.6	0.1676	0.707662 (10)	0.70748	0.1601	0.512386 (9)	0.512307	–4.5	3.49
T59b	323	28	3.02	11.8	0.2553	0.708142 (10)	0.70786	0.1556	0.512347 (9)	0.512269	–5.3	6.10

Thermobarometry

Apatite and zircon saturation temperatures (Harrison and Watson 1983; Watson and Harrison 1983; Hanchar and Watson 2003; Miller et al. 2003) and temperatures based on the hornblende-plagioclase geothermometer (Blundy and Holland 1990; Holland and Blundy 1994) are given in Table 7. Although hornblende is a widely used mineral for thermobarometric studies in calc-alkaline igneous rocks (e.g. Stein and Dietl 2001), it alters easily in most magmatic environments, and the obtained pressures and temperatures do not always reflect the conditions during crystallization.

Within the Torul granitoids both Zr and P concentrations decrease with increasing SiO_2 content (Fig. 6 i, p). With the exception of the quartz diorite, zircon and apatite saturation temperatures range from 850 to 900°C. The temperatures obtained for the quartz diorite are around 800°C. Since zircon and apatite are early crystallizing phases the saturation temperatures may represent near-liquidus relations. Calculated hornblende–plagioclase temperatures (670–760°C) are much lower compared to the zircon and apatite saturation temperatures. This can be explained by the lower closure temperature of hornblende or by subsequent alteration of this mineral. There is evidence for both. Subhedral hornblende crystals in the sample indicate the late-stage crystallization of hornblende and microprobe analysis show that some of the hornblendes are partially altered into tremolites.

The Torul pluton contains the critical mineral assemblage of, quartz + plagioclase + K-feldspar + hornblende + biotite + apatite + zircon + titanite + Fe–Ti oxide, for application of the Al-in-hornblende barometer (Hammarstrom and Zen 1986; Andersen and Smith 1995; Hollister et al. 1987). Using the calibration of Anderson and Schmidt (1995), pressures between 1 and 2.5 kbar were

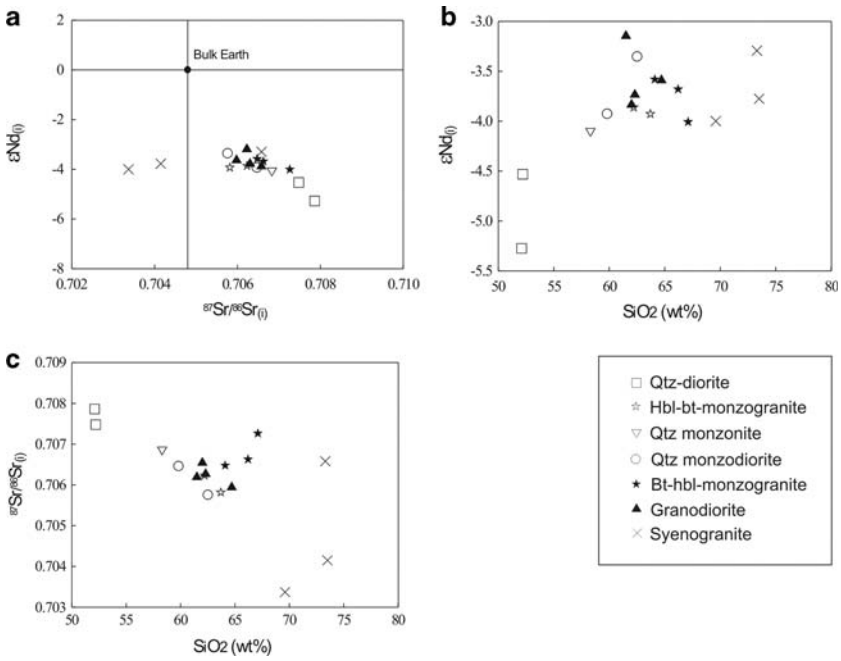

Fig. 9 **a** $\varepsilon_{Nd(i)}$ values versus $^{87}Sr/^{86}Sr_{(i)}$ ratio; **b** and **c** $\varepsilon Nd_{(i)}$ and $^{87}Sr/^{86}Sr_{(i)}$ versus SiO_2, respectively. $\varepsilon_{Nd(i)}$ and $^{87}Sr/^{86}Sr_{(i)}$ values are calculated for an age of 77 Ma

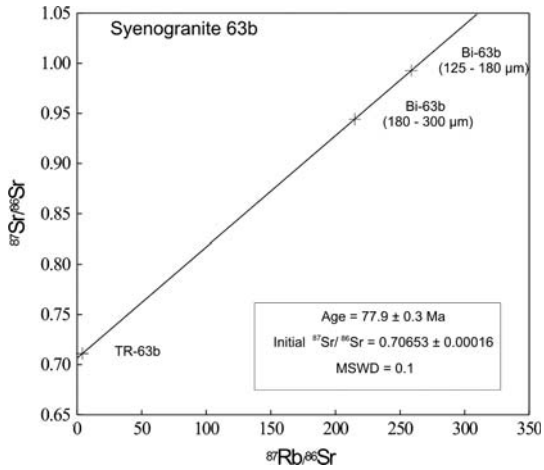

Fig. 10 $^{87}Rb/^{86}Sr$ versus $^{87}Sr/^{86}Sr$ isochron diagram for a whole-rock and two biotite fractions from the syenogranite (sample 63b) of the Torul pluton. *Numbers in brackets* indicate grain size fractions of the biotite concentrates

obtained in the granodiorites, biotite hornblende monzogranites, quartz monzodiorites, quartz monzonites and hornblende biotite monzogranites. These values correspond to emplacement depths between ~3 and 8 km.

Source rocks of the Torul granitoids

Dehydration melting experiments of various source rock lithologies (Patiño Douce and Johnston 1991; Wolf and Wyllie 1994; Patiño Douce and Beard 1996; Patiño Douce and McCarthy 1998) yield partial melts of distinct chemical signatures that allow for discrimination between compositionally different protoliths (Altherr and Siebel 2002; Topuz et al. 2005). Compositional differences of magmas produced by partial melting of different source rocks, such as amphibolites, tonalitic gneisses, metagraywackes, metapelites and amphibolites, under variable melting conditions, may be visualized in terms of molar oxide ratios. Dehydration melting of metapelites and metagreywackes (Rapp et al. 1991; Rapp 1995; Rapp and Watson 1995) yields higher K_2O/Na_2O, Mg#, $Al_2O_3/(FeO_{total} + MgO + TiO_2)$, $(Na_2O + K_2O)/(FeO_{total} + MgO + TiO_2)$ and lower $CaO + FeO_{total} + MgO + TiO_2$ values compared to the investigated rocks (Fig. 12). The chemical composition of the Torul pluton would be broadly compatible with an origin by dehydration melting from mafic lower crustal rocks (e.g. amphibolites). In addition, the syenogranites have slightly higher values of K_2O/Na_2O, $Al_2O_3/(MgO + FeO_{total})$, $Al_2O_3/(FeO_{total} + MgO + TiO_2)$, $(Na_2O + K_2O)/(FeO_{total} + MgO + TiO_2)$, whereas the quartz diorites have slightly higher $Na_2O + K_2O + Al_2O_3 + CaO + FeO_{total} + MgO + TiO_2$ values and Mg# compared to the other rock types in Torul pluton (Fig. 12).

Mode of emplacement

Over the years, various modes of magma ascent and emplacement mechanisms, such as diapirism (Marsh 1982; Bateman 1984), stoping (Daly 1933; Marsh 1982), ballooning (Pitcher and Read 1963; Bateman 1985; Ramsay 1989) and dyking (Petford, 1996; Brown and Tryggvason 2001; Haederle and Atherton 2002) have been identified.

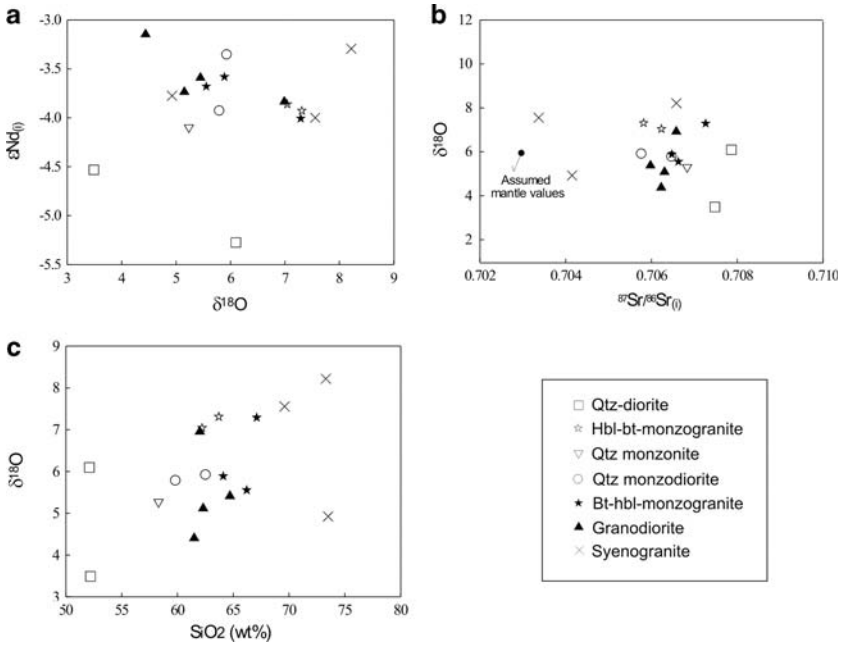

Fig. 11 **a** $\varepsilon_{Nd(i)}$value versus $\delta^{18}O$ isotopic ratio; **b** $\delta^{18}O$ values versus $^{87}Sr/^{86}Sr_{(i)}$; **c** $\delta^{18}O$ versus SiO_2; $\varepsilon_{Nd(i)}$ and $^{87}Sr/^{86}$ $Sr_{(i)}$ values are calculated for an age of 77 Ma

Table 7 Pressure and temperature calculations for granitoids from the Torul pluton obtained from zircon and apatite saturation temperature and plagioclase-hornblende geothermometry

Rock type	Zircon (°C)	Apatite (°C)	Hbl-Pl[a] (°C)	*P* (kbar)[b]
Syenogranite	915 ± 10	878 ± 10	–	–
Granodiorite	888 ± 14	879 ± 10	760 ± 10	2.5 ± 0.5
Bt-hbl-monzogranite	905 ± 10	886 ± 20	720 ± 15	1.4 ± 0.5
Qtz-monzodiorite	893 ± 5	841 ± 11	735 ± 20	0.9 ± 0.3
Qtz-monzonite	891 ± 5	837 ± 15	670 ± 25	1.2 ± 0.4
Hbl-bt-monzogranite	903 ± 10	864 ± 10	680 ± 30	1.7 ± 0.5
Qtz-diorite	793 ± 14	828 ± 10	–	–

Qtz Quartz, *Bt (bt)* Biotite, *Hbl (hbl)* Hornblende, *Pl* Plagioclase

[a] Blundy and Holland (1990) formulation used to calculate temperatures from hornblende-plagioclase pairs. Uncertainties calculated from temperatures estimated from similar composition rocks

[b] Schmidt (1992) formulation used to calculate pressures from hornblendes. Uncertainties calculated from pressures estimated from similar composition rocks

The contacts between the Torul pluton and the country rocks are predominantly sharp and discordant, the contact facies are finer-grained, and the shape of the pluton is elliptic. The textures are massive, porphyritic and granophyric, and the granitoids contain abundant country rock xenoliths at the endocontact. There is a widespread foliation texture developed, especially at the margins of the pluton. All of these features show that the Torul pluton emplaced into shallow crustal depths either by a stoping type of ascent or by ballooning.

It is believed that subduction-related fracture tectonic played an important role during the emplacement of the granitoids within the Pontide magmatic arc (Gedikoğlu 1978). In general, the long axis of most granitic plutons shows good agreement with the major tectonic directions (NE–SW, NW–SE). These directions correspond to the two main fracture alignments in the Eastern Pontides as defined by Bektaş and Çapkınoğlu (1997), suggesting the important role of fractures during pluton emplacement. It seems therefore likely that the Torul pluton emplaced along a NE–SW trending fracture line during the Upper Cretaceous.

Tectonic setting

The Torul granitoids are medium- to high-K, calc-alkaline rocks enriched in LILEs such as Rb, Th, U and K with respect to the HFSEs, especially Nb and Ti (Fig. 8). Apart from the quartz diorite, all rock types show a significant positive Pb anomaly. Magmas with these chemical features are generally believed to be generated in subduction-related environments (e.g. Floyd and Winchester 1975; Rogers and Hawkesworth 1989; Sajona et al. 1996). Applying the discrimination criteria of Pearce et al. (1984), all samples plot in the fields of volcanic arc granites (VAG) and syn-collisional granites (Syn-COLG) in the Nb versus Y diagram (Fig. 13a), whereas in the Rb versus (Y+Nb) diagram, the samples plot in the VAG field (Fig. 13b). Lower-silica samples (quartz diorites, 52–55 wt% SiO_2) fall within the VAG field, whereas the high-silica samples (70–74 wt% SiO_2) plot around the boundary between the

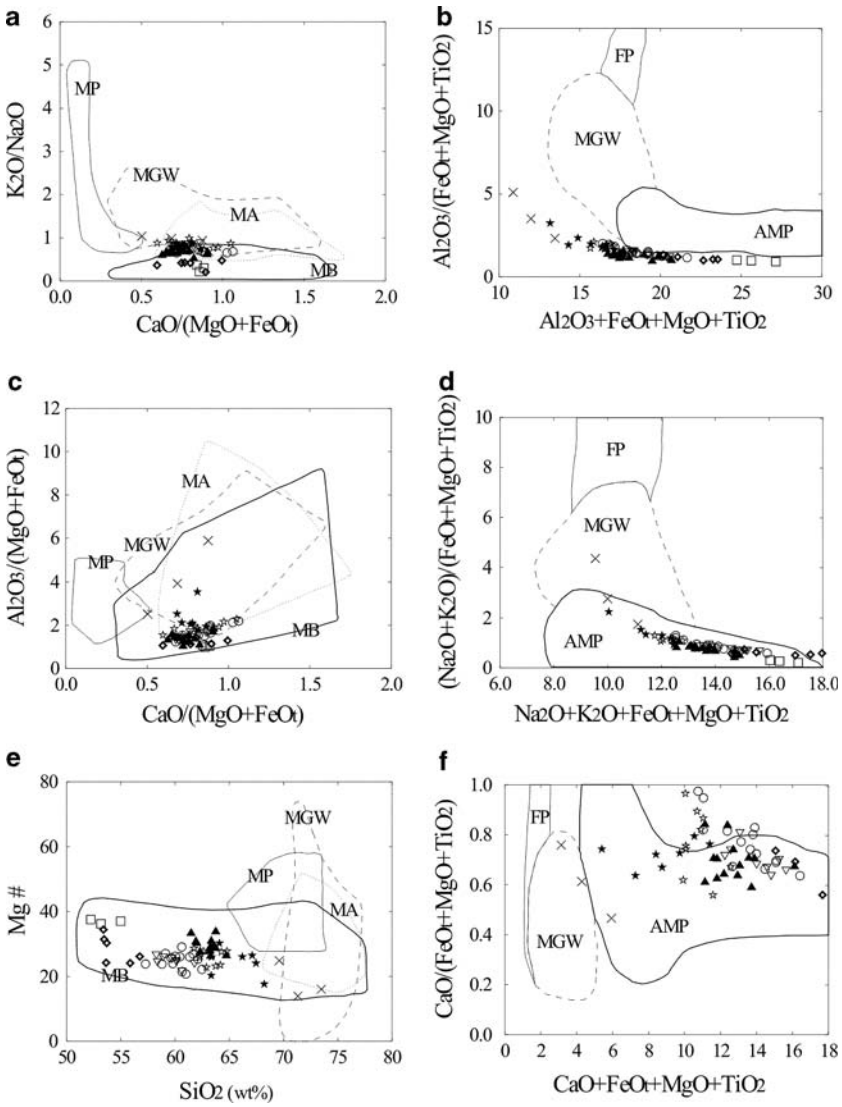

Fig. 12 **a–f** Chemical composition of the Torul granitoids. *Outlined fields* denote compositions of partial melts obtained in experimental studies by dehydration melting of various bulk compositions. *MB* metabasalts (*bold-solid line*); *MA* meta-andesites (*dotted line*); *MGW* metagreywackes (*dashed line*); *MP* metapelites (*solid line*); *AMP* amphibolites (*bold-solid line*). Data sources: Vielzeuf and Holloway (1988), Patiño Douce and Johnston (1991), Rapp et al. (1991), Gardien et al. (1995), Rapp (1995), Rapp and Watson (1995), Patiño Douce and Beard (1996), Stevens et al. (1997), Skjerlie and Johnston (1996), Patiño Douce (1997, 1999), Patiño Douce and McCarthy (1998). See Fig. 3 for explanation

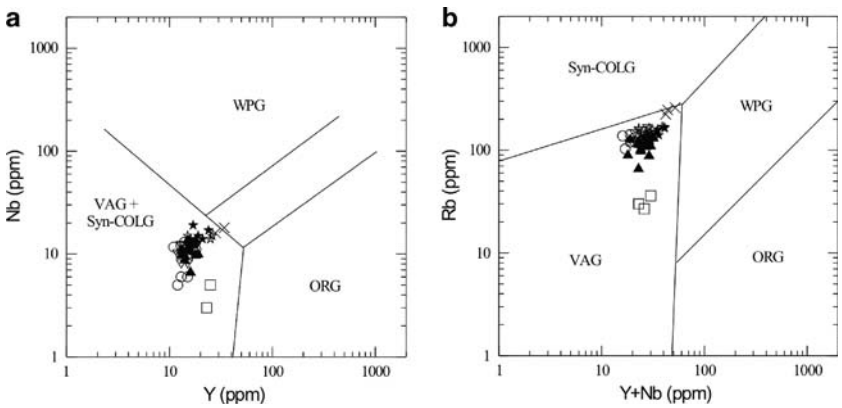

Fig. 13 **a** Nb-Y and **b** Rb-(Y+Nb) discrimination diagrams (Pearce et al. 1984) for samples from the Torul pluton, showing the fields of volcanic-arc granites (*VAG*), syn-collisional granites (*Syn-COLG*), within-plate granites (*WPG*) and ocean-ridge granites (*ORG*). See Fig. 3 for explanation

VAG and COLG fields. This shift is likely due to progressive magma differentiation (Förster et al. 1997).

It has been demonstrated (Brown et al. 1984) that the abundances of incompatible elements in granites can be correlated with the degree of arc maturity. Increase of the Rb/Zr ratio with increasing Nb and Y content is in accordance with the arc maturity, from primitive to mature. A comparison of the Torul pluton with arc-type granitoids is

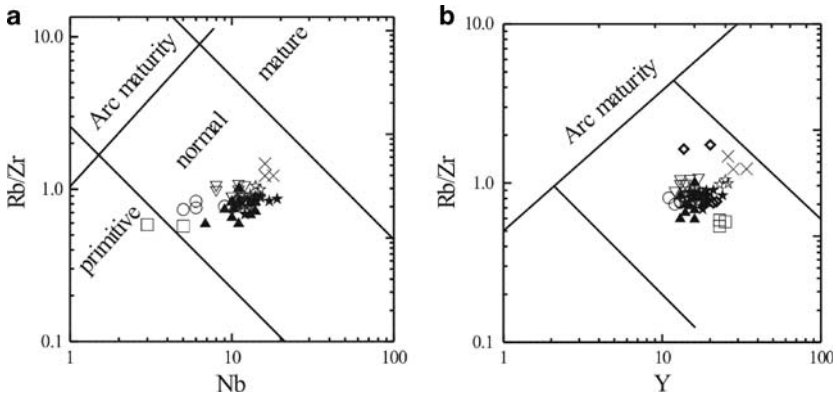

Fig. 14 **a** Nb versus Rb/Zr and **b** Y versus Rb/Zr diagrams (after Brown et al. 1984) for samples from the Torul pluton. See Fig. 3 for explanation

performed on the Nb versus Rb/Zr and Y versus Rb/Zr diagrams (Fig. 14). All rock types from the pluton plot in the normal arc fields (Fig. 14a, b), except the quartz diorites which plot at the primitive arc-normal arc transition (Fig. 14a).

Discussion

The Eastern Pontide belt represents a Mesozoic to Early Cenozoic paleo-subduction zone. The generation of subduction-related granitoids reached a peak during Late Cretaceous to Paleocene. The composition of the granitoids shifts from tonalitic-trondhjemitic through calc-alkaline to alkaline with increasing crustal thickness from Jurassic to Late Eocene (Köprübaşı et al. 2000).

The geochemical features of the Torul pluton (i.e. depletion of Ba, Sr, Nb, and Ti, enrichment of Rb, Th, K, Pb and La) are also compatible to those of typical crustal melts, e.g. granitoids of the Lachlan Fold belt (Chappell and White 1992). Several experimental studies (Wolf and Wyllie 1994; Rapp and Watson 1995) have shown that extremely high temperatures in excess of ~1,100°C are needed to produce mafic metaluminous low-silica (~58 wt%) melts by dehydration melting of metabasic crustal rocks. Such melts are generally characterized by low Mg# (~44) and high Na_2O contents (~4.3 wt %). The Torul intrusions have low Mg# (38 to 14) and high Na_2O contents (2.3–3.8 wt%). Compositional diversity among crustal magmas may arise in part from different source compositions, but variation of intrinsic parameters, such as pressure, temperature, oxygen fugacity, or water content during partial melting also plays an equally important role (e.g. Beard et al. 1994; Wolf and Wyllie 1994; Patiño Douce and Beard 1996; Thompson 1996; Stevens et al. 1997; Altherr et al. 2000). These parameters control the degree of partial melting and the stability fields of residual mineral phases (e.g. plagioclase, biotite, hornblende, orthopyroxene, garnet) that buffer resultant melt composition. Partial melts derived from mafic sources, for example, have lower K_2O/Na_2O, $Al_2O_3/(MgO + FeO_{total})$, Mg#, $Al_2O_3/(FeO_{total} + MgO + TiO_2)$, $(Na_2O + K_2O)/(FeO_{total} + MgO + TiO_2)$, $CaO/(FeO_{total} + MgO + TiO_2)$ and higher $Na_2O + K_2O + Al_2O_3 + CaO + FeO_{total} + MgO + TiO_2$ than those derived from metapelites and metagraywackes as seen in the Torul pluton (Fig. 12).

Trace element characteristics can yield important constraints on the depth of magma segregation and subsequent fractionation processes. Crustal lithologies show a depth-dependent mineralogy. For any fixed bulk-rock composition, the amount of garnet increases and the amount of plagioclase decreases with increasing depth. Certain trace element abundances and ratios can be used as indicators for the relative amounts of garnet, clinopyroxene, hornblende and plagioclase as fractionating phases either during magma segregation from the source region or subsequent fractionation (e.g. Altherr et al. 1999). Fractionation of garnet will lower the relative abundances of HREE, Y, and Sc in the remaining melt phase. Plagioclase fractionation will result in lower abundances of Ba and Sr, low Sr/Nd ratios, and negative Eu anomalies in the chondrite-normalized REE patterns of the melts. Fractionation of hornblende will cause an increase in LREE/HREE in the residual melt, but a concave-upward shape (e.g. Romick et al. 1992) should characterize the resulting chondrite-normalized REE pattern of the melt. The felsic syenogranites (SiO_2-rich) have relatively high abundances of Yb, low abundances of Sr, and low values of Sr/Y, Sr/Nd, Zr/Y, and (Tb/Yb)cn. Chondrite-normalized REE patterns of these samples display variable negative Eu anomalies and are characterized by moderate concave upward shapes (Fig. 7b). These features preclude the presence of substantial amounts of garnet either during partial melting or as part of the fractionating assemblage during an AFC process (DePaolo 1981). Compared to the other rock types the quartz diorites display similar abundances of large ion lithophile elements (LILE), but higher abundances of Sr, lower abundances of Yb, and higher ratios of Sr/Y, Sr/Nd,

Zr/Y and (Tb/Yb)cn. Chondrite-normalized REE patterns of these rocks display slightly negative Eu anomalies and are characterized by minor concave upward shapes (Fig. 7h), implying some feldspar and hornblende fractionation during magma differentiation.

The Torul pluton has textures that indicate magma mingling and mixing processes. The presence of MMEs may indicate mingling of coeval mafic (dioritic) and felsic magmas (e.g. Didier 1973; Vernon 1990; Didier and Barbarin 1991; Barbarin and Didier 1992). Similar mineral assemblages, mineral compositions and existence of strong correlations between major and trace elements show the MME and host granitoids, although concentrations of major and trace elements are different. The resorbed nature of plagioclase megacrysts in the enclaves and the similarity in anorthite contents between these crystals and host rock plagioclase crystals suggest a common origin. Most probably, plagioclase, together with K-feldspar and quartz from the granitic host magma was mechanically transferred to the mafic globules during the hybridization process. Oscillatory-zoned plagioclases (Fig. 4b), coexistence of two types of plagioclase phenocrysts, irregular changes of anorthite contents within plagioclase, poikilitic textures (Fig. 4c, e–g), acicular hornblende, blade and acicular biotite (Fig. 4b), acicular apatite in plagioclase (Fig. 4h), prismatic-cellular plagioclase growth and K-feldspar megacrysts in mafic microgranular enclaves (Barbarin 1988; Lesher 1990; Hibbard 1991; Baxter and Feely 2002) possibly record the mixing of coexisting mafic and felsic magmas. Since original compositions of the enclaves (former globules of mafic melt) were probably modified by interaction with the felsic host magma (as suggested for other occurrences; e.g. Waight et al. 2000), a more thorough discussion of the genesis of the microgranular enclaves is beyond the scope of this study.

Conclusions

The Torul pluton is a composite granitoid pluton which belongs to the medium to high-K, calc-alkaline series. Intrusion contact relationship, mineralogical, geochemical and isotopic characteristics allows defining three major suites. According to their emplacement chronology, these are (1) syenogranites, followed by (2) granodiorites, biotite hornblende monzogranites, quartz monzodiorites, quartz monzonites, hornblende biotite monzogranites and (3) quartz diorites.

The Torul pluton displays fractionated chondrite-normalized REE patterns with pronounced negative Eu anomalies. These features combined with the decrease of Al_2O_3, TiO_2, CaO, MgO, Fe_2O_3, P_2O_5, and Sr with increasing silica suggest that the granitoids have undergone fractionation of plagioclase, amphibole, pyroxene, apatite and titanite. The geochemical and isotopic composition of the Torul pluton is broadly compatible with an origin by dehydration melting from a metabasaltic source.

Major and trace element patterns indicate that the Torul pluton consists of volcanic arc granitoids. The rocks represent a period of (immature) arc development and probably formed during an early stage of convergent plate boundary tectonics. Magmatism is related to subduction of the Neo-Tethyan Ocean beneath the Eurasian plate along the Izmir-Ankara-Erzincan suture zone during the Cretaceous.

Acknowledgments We appreciate the help of E. Reitter and G. Stoschek during radiogenic and stable isotope analyses. Thanks are due to Prof. T. Dunn for microprobe analyses. Prof. M. Arslan is kindly thanked for his general improvement of the manuscript. This work was supported by the Research Fund of Karadeniz Technical University (Project number: 96.112.005.16).

References

Çamur MZ, Güven İH, Er M (1996) Geochemical characteristics of the Eastern Pontide volcanics: An example of multiple volcanic cycles in arc evolution. Turk J Earth Sci 5:123–144

Şahin SY (2005) Transition from arc- to post-collision extensional setting revealed by K–Ar dating and petrology: an example from the granitoids of the Eastern Pontide Igneous Terrane, Araklı-Trabzon, NE Turkey. Geol J 40: 425–440

Şen C, Arslan M, Van A (1998) Geochemical and petrological characteristics of the eastern Pontide Eocene (?) alkaline volcanic province, NE Turkey. Turkish J Earth Sci 7:231–239

Şengör AM, Yılmaz Y (1981) Tethyan evolution of Turkey: a plate tectonic approach. Tectonophysics 75:181–241

Adamia SA, Lordkipanidze MB, Zakariadze GS (1977) Evolution of an active continental margin as exemplified by the Alpine history of the Caucasus. Tectonophysics 40:183–199

Akın H (1978) Geologie, Magmatismus und Lagerstaettenbildung im ostpontischen Gebirge-Türkei aus der Sicht der Plattentektonik. Geol Rundsch 68:253–283

Akıncı ÖT (1984) The Eastern Pontide volcano-sedimentary belt and associated massive sulphide deposits. In: Dixon JE, Robertson AHF (eds) The geological evolution of the Eastern Mediterranean, vol 17. Geological Soc London Special Publication, London, pp 415–428

Altherr R, Siebel W (2002) I-type plutonism in a continental back-arc setting: Miocene granitoids and monzonites from the central Aegean Sea, Greece. Contrib Mineral Petrol 143:397–415

Altherr R, Henjes-Kunst F, Langer C, Otto J (1999) Interaction between crustal-derived felsic and mantle-derived mafic magmas in the Oberkirch pluton (European Variscides, Schwarzwald, Germany). Contrib Mineral Petrol 137:304–322

Altherr R, Holl A, Hegner E, Langer C, Kreuzer H (2000) High potassium, calc-alkaline I-type plutonism in the European Variscides: northern Vosges (France) and northern Schwarzwald (Germany). Lithos 50:51–73

Anderson JL, Smith DR (1995) The effects of temperature and oxygen fugacity on the Al-in-hornblende barometry. Am Mineral 80:549–559

Arslan M, Aslan Z (2005) Mineralogy, petrography and whole-rock geochemistry of the Tertiary granitic intrusions in the Eastern Pontides, Turkey. J Asian Earth Sci 27:177–193

Arslan M, Tüysüz N, Korkmaz S, Kurt H (1997) Geochemistry and petrogenesis of the eastern Pontide volcanic rocks, Northeast Turkey. Chemie der Erde 57:157–187

Arslan M, Şen C, Aliyazıcıoğlu İ, Kaygusuz A, Aslan Z (2000) Trabzon ve Gümüşhane yörelerinde (KD, Türkiye) yüzeylenen Eosen (?) volkanitlerinin karşılaştırmalı jeolojisi, mineralojisi ve petrolojisi. Yerbilimleri ve Madencilik Kongresi Bildiriler Kitabı, vol 1, pp 39–53

Arslan M, Kolaylı H, Temizel İ (2004) Petrographical, geochemical and petrological characteristics of the Güre (Giresun, NE Turkey) Granitoid. Bull Earth Sci Appl Res Centre Hacettepe Univ 30:1–21

Barbarin B (1988) Field evidence for successive mixing and mingling between the Piolard Diorite and the Saint-Julien-La-Vetre Monzogranite (Nord-Forez, Massif Central, France). Can J Earth Sci 25:49–59

Barbarin B (1999) A review of the relationships between granitoid types, their origins and their geodynamic environments. Lithos 46:605–626

Barbarin B, Didier J (1992) Genesis and evolution of mafic microgranular enclaves through various types of interaction between coexisting felsic and mafic magmas. Trans R Soc Edinb Earth Sci 83:145–153

Bateman R (1984) On the role of diapirism in the segregation, ascent and final emplacement of granitoid magmas. Tectonophysics 110:211–231

Bateman R (1985) Aureole deformation by flattening around a diapir during in-situ ballooning: the Cannibal Creek granite. J Geol 93:293–310

Baxter S, Feely M (2002) Magma mixing and mingling textures in granitoids: examples from the Galway Granite, Ireland. Mineral Petrol 76:63–74

Beard JS, Lofgren GE, Sinka AK, Tollo RP (1994) Partial melting of apatite-bearing charnockite, granulite, and diorite: melt compositions, restite mineralogy, and petrologic implications. J Geophys Res 99:21591–21604

Bektaş O, Çapkınoğlu Ş (1997) Doğu Pontid magmatik arkında (KD Türkiye) neptüniyen dayklar ve blok tektoniği, Mesozoyik havzaların kinematiği ile ilgili bulgular. ÇÜ 20.Yıl Sempozyumu, Adana, Bildiri Özleri, pp 187–189

Bektaş O, Şen C, Atıcı Y, Köprübaşı N (1999) Migration of the Upper Cretaceous subduction-related volcanism towards the back-arc basin of the eastern Pontide magmatic arc (NE Turkey). Geol J 34:95–106

Blundy JD, Holland, TJB (1990) Calcic amphibole equilibria and a new amphibole-plagioclase geothermometer. Contrib Mineral Petrol 104:208–224

Boztuğ D, Kuşçu İ, Erçin Aİ, Avcı N, Şahin SY (2003) Mineral deposits associated with the pre-, syn- and post-collisional granitoids of the neo-Tethyan convergence system between the Eurasian and Anatolian plates in NE and Central Turkey. In: Eliopoulops D et al (eds) Mineral exploration and sustainable development. Millpress, Rotterdam, pp 1141–1144

Boztuğ D, Jonckheere R, Wagner GA, Yeğingil Z (2004) Slow Senonian and fast Palaeocene–Early Eocene uplift of the granitoids in the Central Eastern Pontides, Turkey: apatite fission-track results. Tectonophysics 382:213–228

Boztuğ D, Erçin Aİ,Kuruçelik MK, Göç D, Kömür İ, İskenderoğlu A (2006) Geochemical characteristics of the composite Kaçkar batholith generated in a Neo-Tethyan convergence system, Eastern Pontides, Turkey. J Asian Earth Sci, pp 1–17 (in press)

Brown D, Tryggvason A (2001) Ascent mechanism of the Dzabyk batholith, southern Urals: constraints from the URSEIS reflection seismic profiling. J Geol Soc 158:881–884

Brown GC, Thorpe RS, Webb PC (1984) The geochemical characteristics of granitoids in contrasting arcs and comments on magma sources. J Geol Soc 141:413–426

Chappell BW, White AJR (1974) Two contrasting granite types. Pac Geo 8:173–174

Chappell BW, White AJR (1992) I- and S-type granites in the Lachlan Fold Belt. Trans R Soc Edinb Earth Sci 83:1–26

Clarke DB (1992) Granitoid rocks. Chapman& Hall, London, p 283

Clayton RN, Mayeda TK (1963) The use of bromine pentaflouride in the extraction of oxygen from oxides and silicates for isotopic analysis. Geo Cosmoc Acta 27:43–45

Daly RA (1933) Igneous rocks and the depths of the Earth: McGraw-Hill (Hofner Reprint 1962), New York, pp 598

Debon F, Le Fort P (1982) A chemical-mineralogical classification of common plutonic rocks and associations. Trans R Soc Edinb Earth Sci 73:135–149

Delaloye M, Çoğulu E, Chessex R (1972) Etude ge'ochronometrique des massifs cristallins de Rize et de Gümüşhane, Pontides Orientales (Turquie). CR des Sciences, vol 7/2–3. SPHN, Geneve, pp 43–52

DePaolo DJ (1981) Trace element and isotopic effects of combined wallrock assimilation and fractional crystallization. Earth Planet Sci Lett 53:189–202

Didier J (1973) Granites and their enclaves. Elsevier, London, p 393

Didier J, Barbarin B (1991) Enclaves and granite petrology: developments in petrology, vol 13. Elsevier, Amsterdam, 625 pp

Eğin D, Hirst DM, Phillips R (1979) The petrology and geochemistry of volcanic rocks from the northern Harşit river area, Pontide volcanic province, northeast Turkey. J Volcan Geotherm Res 6:105–123

Ercan T, Gedik A (1983) Pontidlerdeki volkanizma. Jeoloji Mühendisliği Dergisi 18:3–30

Förster HJ, Tischendorf G, Trumbull RB (1997) An evalution of Rb vs. (Y+Nb) discrimination diagram to infer tectonic setting of silicic igneous rocks. Lithos 40:261–293

Floyd PA, Winchester JA (1975) Magma type and tectonic setting discrimination using immobile elements. Earth Planet Sci Lett 27:211–218

Galan G, Pin C, Duthon JL (1996) Sr–Nd isotopic record of multistage interactions between mantle derived magmas and crustal components in a collision context: the ultramafic-granitoid association from Vivero (Hercynian belt, NW Spain). Chem Geol 131:67–91

Gardien V, Thompson AB, Grujic D, Ulmer P (1995) Experimental melting of biotite+plagioclase+quartz ± muscovite assemblages and implications for crustal melting. J Geophys Res 100:15581–15591

Gedik A, Ercan T, Korkmaz S, Karataş S (1992) Rize-Fındıklı Çamlıhemşin arasında (Doğu Karadeniz) yer alan magmatik kayaçların petrolojisi ve Doğu Pontidlerdeki bölgesel yayılımları. Türkiye Jeoloji Bülteni 35:15–38

Gedikoğlu A (1978) Harşit granit karmaşığı ve çevre kayaçları, Doçentlik Tezi, K.T.Ü, Yer Bilimleri Fakültesi, Trabzon

Genç ŞC, Yılmaz Y (1995) Post collisional Eocene magmatic activity of NW Anatolia: EUG VII, 9–13 April, Strasbourg. Terra Abstracts, Terra Nova, vol 7, pp 181

Giles DL (1974) Geology and mineralization of the Ulutaş copper–molybdenum prospect, mineral exploration in two areas. UNDP Technical Report, 6, MTA, Ankara (unpublished)

Güven İH (1993) Doğu Pontidler'in 1/ 250 000 ölçekli kompilasyonu, MTA. Genel Müdürlüğü, Ankara

Haederle M, Atherton MP (2002) Shape and intrusion style of the Coastal Batholith, Peru. Tectonophysics 345:17–28

Hammastrom JM, Zen EA (1986) Aluminum in hornblende: an empirical igneous geobarometer. Am Mineral 71:1297–1313

Hanchar JM, Watson EB (2003) Zircon saturation thermometry. In: Hanchar JM, Hoskin PWO (eds) Zircon. Rev in mineralogy and geochemistry, vol 53. Mineralogical Society of America, Geochemical Society of America, pp 89–112

Harmon RS, Hoefs J (1995) Oxygen isotope heterogeneity of the mantle deduced from global ^{18}O systematics of basalts from different geotectonic settings. Contrib Mineral Petrol 120:95–114

Harrison TM, Watson EB (1983) Kinetics of zircon dissolution and zirconium diffusion in granitic melts of variable water content. Contrib Mineral Petrol 84:66–72

Hibbard MJ (1991) Textural anatomy of twelve magma-mixed granitoid systems. In: Didier J, Barbarin B (eds) Enclaves and granite petrology, developments in petrology, vol 13. Elsevier, Amsterdam, pp 431–444

Holland TJB, Blundy JD (1994) Non-ideal interaction in calcic amphiboles and their bearing on amphibole-plagioclase thermometry. Contrib Mineral Petrol 116:433–447

Hollister LS, Grissom GC, Peters EK, Stowell HH, Sisson VB (1987) Confirmation of the empirical correlation of Al in hornblende with pressure of solidification of calc-alkaline plutons. Am Mineral 72:231–239

Jica (1986) The republic of Turkey report on the cooperative mineral exploration of Gümüşhane area, consolidated report. Japan Int Coop Agency, 146 pp

Karslı O (2002) Granitoyid kayaçlarda magma etkileşimleri için petrografik, mineralojik ve kimyasal bulgular: Dölek ve Sarıçiçek Plütonları (Gümüşhane-KD Türkiye), PhD Thesis, Karadeniz Technical University, Trabzon

Kaygusuz A (2000) Torul ve çevresinde yüzeylenen kayaçların petrografik ve jeokimyasal incelenmesi. PhD Thesis, KTÜ-Trabzon, 23 pp

Kaygusuz A, Şen C (1998) Torul (Gümüşhane) granitoyidinin petrografik ve kimyasal karakterleri, Fırat Üniversitesinde Jeoloji Mühendisliği Eğitiminin 20. Yılı Sempozyumu Bildirileri, pp 381–388

Kazmin VG, Sbortshikov IM, Rıcou LE, Zonenshain LP, Boulin J, Knıpper A (1986) Volcanic belts as markers of the Mesozoic-Cenozoic evolution of Tethys. Tectonophysics 123:123–152

Kazmin VG, Schreider AA, Bulychev AA (2000) Early stages of evolution of the Black Sea. In: Bozkurt E, Winchester JA, Piper JDA (eds) Tectonics and magmatism in Turkey and surrounding area, vol 173. Geological Society London, Special Publications, pp 235–249

Ketin İ (1966) Tectonic units of Anatolia (Asia Minor). Maden Tetkik ve Arama Bulletion 66:22–34

Köprübaşı N, Şen C, Kaygusuz A (2000) Doğu Pontid adayayı granitoyidlerin karşılaştırılmalı petrografik ve kimyasal özellikleri, Uygulamalı Yerbilimleri 1:111–120

Korkmaz S, Tüysüz N, Er M, Musaoğlu A, Keskin İ (1995) Stratigraphy of the Eastern Pontides, NE Turkey. In: Erler et al. (eds) Procedings of the international symposium of the geology of the Black Sea Region, pp 59–69

Le Maitre RW, Bateman P, Dudek A, Keller J, Lameyre J, Le Bas MJ, Sabine PA, Schmid R, Sorensen H, Streckeisen A, Wooley AR, Zanettin B (1989) A classification of igneous rocks and glossary of terms. Blackwell, Oxford, p 193

Lesher CE (1990) Decoupling of chemical and isotopic exchange during magma mixing. Nature 344:235–237

Marsh BD (1982) On the mechanics of igneous diapirism, stoping and zone melting. Am J Sci 282:808–855

Miller CF, Meschter McDowell S, Mapes RW (2003) Hot and cold granites? Implications of zircon saturation temperatures and preservation of inheritance. Geology 31:529–532

Moore WJ, Mckee EH, Akıncı Ö (1980) Chemistry and chronology of plutonic rocks in the Pontid mountains, northern Turkey. Symposium of European Copper Deposits, Belgrade 1980, pp 209–216

Okay A, Şahintürk Ö (1997) Geology of the Eastern Pontides. In: Robinson AG (ed) Regional and petroleum geology of the Black Sea and surrounding region. AAPG Memoir 68:291–311

Patiño Douce AE (1997) Generation of metaluminous A-type granites by low-pressure melting of calc-alkaline granitoids. Geology 25:743–746

Patiño Douce AE (1999) What do experiments tell us about the relative contributions of crust and mantle to the origin of granitic magmas? In: Castro A, Fernandez C, Vigneresse JL (eds) Understanding granites: intergrating new and classical techniques, vol 168. Geological Society London Special Publication, pp 55–75

Patiño Douce AE, Beard JS (1996) Effects of P, f (O_2) and Mg/Fe ratio on dehydration melting of model metagreywackes. J Petrol 37:999–1024

Patiño Douce AE, Johnston AD (1991) Phase equilibria and melt productivity in the pelite system: implications for the origin of peraluminous granitoids and aluminous granulites. Contrib Mineral Petrol 107:202–218

Patiño Douce AE, McCarthy TC (1998) Melting of crustal rocks during continental collision and subduction. In: Hacker BR, Liou JG (eds) When continents collide: geodynamics and geochemistry of ultra-high pressure rocks. Kluwer, Dordrecht, pp 27–55

Pearce JA, Harris NBW, Tindle AG (1984) Trace element discrimination diagram for the tectonic interpretation of granitic rocks. J Petrol 25:956–983

Peccerillo R, Taylor SR (1976) Geochemistry of Eocene calc-alkaline volcanic rocks from the Kastamonu area, northern Turkey. Contrib Mineral Petrol 58:63–81

Petford N (1996) Dykes or diapirs? Trans R Soc Edinb Earth Sci 87:105–114

Pitcher WS, Read HH (1963) Contact metamorphism in relation to manner of emplacement of the granites of Donegal, Ireland. J Geol 71:261–296

Ramsay JG (1989) Emplacement kinematics of a granite diapir: the Chindamore Batholith, Zimbabwe. J Struct Geol 11:191–209

Rapp RP (1995) Amphibole-out phase boundary in partially melted metabasalt, its control over liquid fraction and composition, and source permeability. J Geophys Res 100:15601–15610

Rapp RP, Watson EB (1995) Dehydration melting of metabasalt at 8–32 kbar: implications for continental growth and crust-mantle recycling. J Petrol 36:891–931

Rapp RP, Watson EB, Miller CF (1991) Partial melting of amphibolite eclogite and the origin of Archean trondhjemites and tonalites. Precambrian Res 51:1–25

Roberts MP, Clemens JD (1993) Origin of high-potassium, calc-alkaline, I-type granitoids. Geology 21:825–828

Robinson AG, Banks CJ, Rutherford MM, Hirst JPP (1995) Stratigraphic and structural development of the eastern Pontides, Turkey. J Geol Soc Lond 152:861–872

Rogers G, Hawkesworth CJ (1989) A geochemical traverse across the North Chilean Andes: evidence for crust generation from the mantle-wedge. Earth Planet Sci Lett 91:271–285

Romick JD, Kay SM, Kay RW (1992) The influence of amphibole fractionation on the evolution of calc-alkaline andesite and dacite tephra from the Central Aleutians, Alaska. Contrib Mineral Petrol 112:101–118

Sajona FG, Maury RC, Bellon H, Cotton J, Defant M (1996) High field strength element enrichment of Pliocene-Pleistocene Island Arc Basalts, Zamboanga Peninsula, western Mindanao (Philippines). J Petrol 37:693–726

Schmidt MW (1992) Amphibole composition in tonalite as a function of pressure: an experimental calibration of the Al-in-hornblende

barometer at 650°C, 3.5 kbar. Contrib Mineral Petrol 110:304–310

Shand SJ (1947) Eruptive rocks. Their genesis, composition, classification and their relation to ore-deposits, 3rd edn. Wiley, New York, p 488

Siebel W, Reitter E, Wenzel T, Blaha U (2005) Sr isotope systematics of K-feldspar in plutonic rocks revealed by the Rb-Sr microdrilling technique. Chem Geol 222:183–199

Skjerlie KP, Johnston AD (1996) Vapour-absent melting from 10 to 20 kbar of crustal rocks that contain multiple hydrous phases: implications for anatexis in the deep to very deep continental crust and active continental margins. J Petrol 37:661–691

Stein E, Dietl C (2001) Hornblende thermobarometry of granitoids from the Central Odenwald (Germany) and their implications for the geotectonic development of the Odenwald. Mineral Petrol 72:185–207

Stevens G, Clemens JD, Droop GTR (1997) Melt production during granulite facies anatexis: experimental data from 'primitive' metasedimentary protoliths. Contrib Mineral Petrol 128:352–370

Streckeisen A (1976) To each plutonic rock its proper name. Earth Sci Rev 12:1–33

Sun SS, McDonough WF (1989) Chemical and isotope systematics of oceanic basalts; implication for mantle compositions and processes. In: Saunders AD, Nory MJ (eds) Magmatism in the ocean basins, vol 42. Geological Society London Special Publication, pp 313–345

Taner MF (1977) Etuda géologique et pétrographique de la région de Güneyce-İkizdere, située au sud de Rize (Pontides orientales, Turquie). PhD Thesis, Universite de Geneve, 180 pp (unpublished)

Taylor SR, McLennan SM (1985) The continental crust: its composition and evolution. Blackwell, Oxford, p 312

Thompson AB (1996) Fertility of crustal rocks during anatexis. Trans R Soc Edinb Earth Sci 87:1–10

Thompson AB, Connolly JAD (1995) Melting of the continental crust: some thermal and petrological constraints on anatexis in continental collision zones and other tectonic settings. J Geophys Res 100:15565–15579

Tokel S (1977) Doğu Karadeniz Bölgesi'nde Eosen yaşlı kalk alkalen andezitler ve jeotektonizma. Türkiye Jeoloji Kurumu Bülteni 20:49–54

Topuz G, Alther R, Schwarz WH, Siebel W, Satır M, Dokuz A (2005) Post-collisional plutonism with adakite-like signatures: the Eocene Saraycık granodiorite (Eastern Pontides, Turkey). Contrib Mineral Petrol 150:441–455

Vernon RH (1990) Crystallization and hybridism in microgranitoid enclave magmas: microstructural evidence. J Geophys Res 95:17849–17859

Vielzeuf D, Holloway JR (1988) Experimental determinations of the fluid-absent melting reactions in the pelitic system. Contrib Mineral Petrol 98:257–276

Waight TE, Dean AA, Maas R, Nicholls IA (2000) Sr and Nd isotopic investigations towards the origin of feldspar megacrysts in microgranular enclaves in two I-type plutons of the Lachlan Fold Belt, southeast Australia. Aust J Earth Sci 47:1105–1112

Watson EB, Harrison TM (1983) Zircon saturation revisited: temperature and composition effects in a variety of crustal magma types. Earth Planet Sci Lett 64:295–304

Wolf M, Wyllie P (1994) Dehydration melting of solid amphibolite at 10 kb: the effect of temperature and time. Contrib Mineral Petrol 115:369–383

Wyllie PJ, Cox KG, Biggar GM (1962) The habit of apatite in synthetic systems and igneous rocks. J Petrol 3:238–243

Yılmaz Y (1981) Sakarya kıtası güney kenarının tektonik evrimi. İstanbul Üniversitesi Yerbilimleri Dergisi 1:33–52

Yılmaz S, Boztuğ D (1996) Space and time relations of three plutonic phases in the Eastern Pontides, Turkey. Int Geol Rev 38:935–956

Yılmaz S, Boztuğ D (1997) Dereli-Şebinkarahisar (Giresun güneyi) arasında yüzeylenen Doğu Pontid plütonizması petrojenezinde magma karışımı, fraksiyonel kristalleşme, kabuksal kirlenme ve kısmi erime süreçleri. Geosound/Yerbilimleri, Çukurova Üniversitesinde Jeoloji Mühendisliği Eğitiminin 20. Yılı Sempozyumu, Özel Sayı 30:833–853

Yılmaz A, Adamia S, Chabukiani A, Chkhotua T, Erdoğan K, Tuzcu S, Karabıyıkoğlu M (2000) Structural correlation of the southern Transcaucasus (Georgia)-Eastern Pontides (Turkey). In: Bozkurt E, Winchester JA, Piper JDA (eds) Tectonics and magmatism in turkey and surrounding area, vol 173. Geological Society London Special Publication, pp 171–182

Yeğingil Z, Boztuğ D, Er M, Oddone M, Bigazzi G (2002) Timing of neotectonic fracturing by fission-track dating of obsidian infilling faults in the İkizdere-Rize area, NE Black Sea region Turkey. Terra Nova 14(3):169–174

Zorpi MJ, Coulon C, Orisini JB (1991) Hybridization between felsic and mafic magmas in calc-alkaline granitoids: a case study in northern Sardinia, Italy. Chem Geol 92:45–86